Erosion and Deposition of Multiple Grain Sizes in a Landscape Evolution Model

by

Nicole M. Gasparini

Submitted to the Department of Civil and Environmental Engineering
in partial fulfillment of the requirements for the degree of

Master of Science in Civil and Environmental Engineering

at the

MASSACHUSETTS INSTITUTE OF TECHNOLOGY

May 1998

Author .....
Department of Civil and Environmental Engineering
May 8, 1998

Certified by .....
Rafael L. Bras
Professor
Thesis Supervisor

Accepted by .....
Joseph Sussman
Chairman, Department Committee on Graduate Students

Erosion and Deposition of Multiple Grain Sizes in a Landscape Evolution Model

by

Nicole M. Gasparini

Submitted to the Department of Civil and Environmental Engineering
on May 8, 1998, in partial fulfillment of the
requirements for the degree of
Master of Science in Civil and Environmental Engineering

Abstract

This work investigates how multiple grain sizes affect sediment transport and deposition in a river basin. A physically based landscape evolution model is modified to account for a sediment mixture of sand and gravel. Bedload transport equations developed by P. Wilcock for sand and gravel mixtures govern erosion and deposition of the two fractions individually. An active layer is used to track the composition of sediment in the bed and a layering algorithm tracks the texture of sedimentary layers below. A layer of parent material which has the same texture across the entire basin replenishes the active layer when there are no sedimentary layers. Basins evolve to steady state through uplift, diffusion (which does not contribute to sorting), and fluvial erosion.

The morphology of basins with a single effective grain size is first investigated. Basin concavity is found to increase with effective grain size. A second set of experiments examines surface texture and morphology in basins with different parent material textures. The results show a systematic increase in the percentage of fine material in the active layer as drainage area increases. This pattern of fining in the active layer is maintained in an equilibrium state, reflecting the natural adjustment between stream gradient, shear stress, and active layer composition. The texture of the active layer differs from the texture of the substrate and is supported by a graphical solution of the equilibrium sediment transport conditions. Basin morphology is not significantly affected by changes in the parent material, due to the adjustment of active layer texture. A third experiment investigates changes in a basin due to a change from dry to wet climate. The results show that the transient state of the landscape is quite different from the final equilibrium, and that both differ in fining pattern and morphology from the initial basin. During the transient state a coarse layer of sediment is buried below the active layer as a result of the climate change.

Thesis Supervisor: Rafael L. Bras
Title: Professor

Acknowledgments

This research was supported by the U.S. Army Construction Engineering Research Laboratory (agreement DACA88-95-R-0020); this support is gratefully acknowledged.

My deepest thanks to Rafael Bras for his constant support and patience. I thank Greg Tucker for working with me during some of my most neurotic states and patiently answering all of my questions, sometimes more than once.

I thank Jennifer Abate, Gretchen Jehle, Amy Johnson, Colleen Kelley, and Monica Ogra for their countless emails, cards, calls, visits and most importantly, their long lasting friendships. I thank my friends Karen Friedman, Guiling Wang, Jenny Jay, and Rachel Adams for being there for me to talk, laugh, and cry with. Finally, I thank my mom, dad and brother, Lucille, Marino, and Francis Gasparini for their encouragement and love.

Contents

List of Figures

List of Tables

Chapter 1

Introduction

Numerical models have enhanced the study of geomorphology, which has traditionally been a field based discipline. This study capitalizes on recent advances, using a physically based numerical model to investigate sediment sorting within an entire drainage basin and the effect of sediment sorting on basin morphology.

Multiple grain sizes have been ignored in previous landscape evolution models (e.g. Willgoose et al. (1989) and Tucker (1996)). Studies have investigated changing the effective grain size of the sediment (Tucker and Bras 1997); however, sediment with multiple grain sizes has yet to be added to landscape evolution models.

A number of numerical channel models have used a distribution of sizes to represent the texture of sediments on the surface of the bed and in the parent material below (e.g. van Niekerk et al. (1992)). These models have been used to investigate changes in grain size in a single-thread channel. Although useful, these two-dimensional models can only address a piece of the system in isolation. The interaction between a channel and the surrounding hillslopes and tributaries, which provide a channel with both sediment and fluvial discharge, can not be captured in these two-dimensional models. The modeling study presented here builds on both landscape evolution models and channel models by adding sediment texture to a three-dimensional model.

Both field and laboratory experiments have investigated controls on surface texture and local slope. Sedimentary deposits which have been laid down over thousands

of years can be viewed in the field, but the controls which produced these deposits can only be inferred. On the other hand, in the laboratory one can watch a system evolve and note exactly what causes different textures on the surface or in deposits below, but both time and space are limited. A numerical model such as the one developed for this study serves to validate hypotheses about the processes which cause the textural patterns observed in large natural systems over geologic time-scales. It can also be used to predict changes in the landscape which might result from environmental changes, such as climate change or deforestation.

Previous field and laboratory studies of heterogeneous sediment transport are discussed in Chapter 2. The sediment transport equations and method for determining critical shear stress developed by Wilcock (1997) and used in this model are described in Chapter 2. Chapter 3 gives a brief overview of GOLEM (Tucker 1996), a previously developed landscape evolution model. The discussion focuses on the changes made to the sediment transport algorithm to accommodate multiple grain sizes. The algorithm developed to track the surface texture and create sedimentary layers is also described in detail.

Chapter 4 discusses basin concavity in five basins with a single effective grain size which were evolved to dynamic equilibrium. The results show that basin concavity increases with effective grain size. Chapter 5 discusses five heterogeneous basins with different parent material textures which were evolved to dynamic equilibrium. In contrast to the homogeneous basins, concavity in the heterogeneous basins does not depend on parent material texture, due to the adjustment of the active layer texture. Downstream fining is produced in all of the heterogeneous basins in dynamic equilibrium. A graphical solution of the sediment transport equations supports the pattern of fining in the basins.

A preliminary study of climate change in a basin with heterogeneous sediment is presented in Chapter 6. Climate change is modeled by increasing the effective precipitation rate in a basin which has reached dynamic equilibrium. From this experiment a number of interesting changes result. The surface texture and basin concavity quickly adjust, quite dramatically, to the increase in precipitation rate.

When the basin reaches a new equilibrium, further modifications are made to the texture of surface sediments and concavity, different from the initial changes. Alluvial sedimentary deposits record the complex changes in the fluvial system caused by the change in climate. This study represents only the first of many different climate change experiments which can be made with this model.

Chapter 2

Review of Heterogeneous Transport Studies

This chapter reviews a number of different studies of heterogeneous sediment transport. It introduces the sand and gravel bedload equations and the method for determining critical shear stress which are used in this modeling study.

2.1 Background

Empirical studies have investigated bedload transport of both single and multiple grain sizes. Describing heterogeneous sediment transport is difficult because the critical shear stress for individual sizes is hard to determine. However, critical shear stress in a homogeneous material has been well described by the Shields curve. Shields (1936) developed an empirical curve of dimensionless critical shear stress for motion of homogeneous sediment (Shields parameter) as a function of grain Reynolds number. Shields parameter or θ, is calculated as

$$\theta = \frac{\tau_c}{(\rho_s - \rho)gD} \tag{2.1}$$

where τ_c is the critical shear stress necessary to entrain a particle of diameter D; ρ_s and ρ are the sediment and water densities, respectively; and g is gravitational

acceleration. Grain Reynolds number is denoted as $Re_* = u_{*c}D/\nu$, where $u_{*c} = \sqrt{\tau_c/\rho}$ is the shear velocity, and ν is the water viscosity. Shields' original plot is often seen recast as critical shear stress versus grain diameter (Figure 2-1) and it is widely used in this form for determining entrainment of particles from a homogeneous bed.

On a heterogeneous bed, the critical shear stress to entrain a given size particle depends not only on the size of the particle itself, but also on the distribution of particle sizes on the bed. The interaction between particles complicates the entrainment process, partly through "hiding and protrusion" of grains (Figure 2-2). The critical shear stress necessary to entrain smaller particles increases due to the presence of larger grains which act to hide the smaller particles. Conversely, in a mixture, large grains tend to protrude above the bed surface more so than they would on a homogeneous bed. This allows large particles to be more easily entrained and hence decreases the critical shear stress needed for motion of large particles. These interactions are not easy to explain quantitatively. Many studies have attempted to quantify the critical shear stress necessary for entrainment of grains in a mixture, but currently there is no universal function to describe critical shear stress in a mixture of sediment sizes.

Wiberg and Smith (1987) developed a quasi-analytical equation for determining critical shear stress of both uniform and mixed sized sediments. Their equation is extremely useful because it works under a wide range of conditions. However the amount of data needed for the calculation limits its applicability in numerical modeling studies.

2.1.1 Equal Mobility

The idea of equal mobility was popularized by Gary Parker and others (Parker and Klingeman (1982); Parker et al. (1982)). Equal mobility is usually observed in gravel bed streams which develop a coarse surface pavement that is immobile for most of the year. When flow conditions permit entrainment of pavement particles, the finer material of the substrate is exposed and made available for transport. All grain sizes are entrained at the same critical shear stress. If equal mobility holds, the total

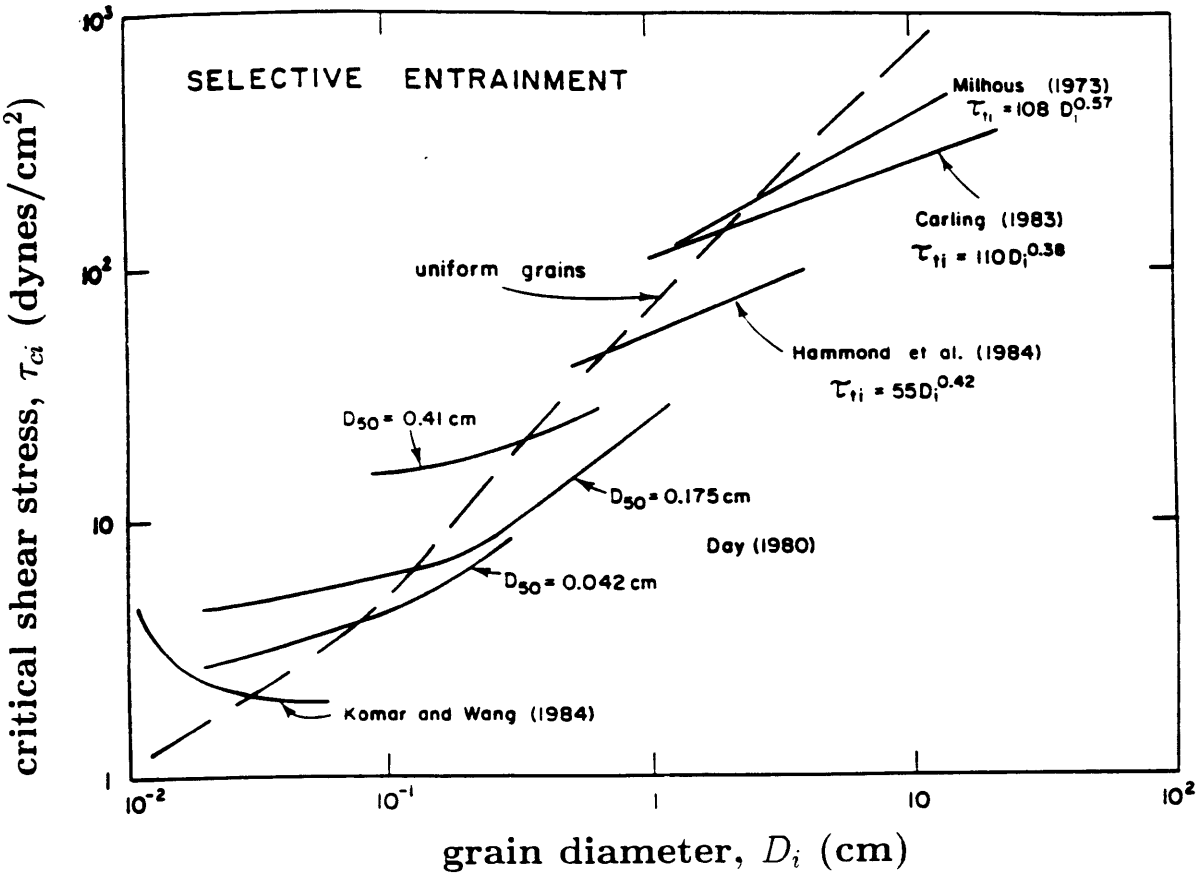

Figure 2-1: Critical shear stress values for different mixtures, taken from Komar (1987). The dashed line represents the Shields curve for particles on a homogeneous bed.

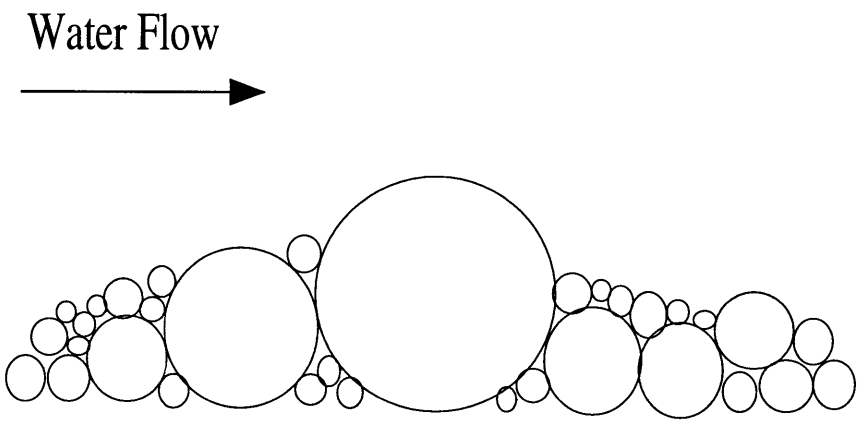

Figure 2-2: Example of a heterogeneous bed.

bedload, to a first order approximation, can be modeled as a function of shear stress and the median grain size, D_{50}, of the subpavement. Equal mobility was found to be satisfactory for determining the size distribution of the mean annual bedload; however lower flows favor smaller grain sizes in the bedload, and higher flows favor larger grain sizes in the bedload (Parker et al. 1982).

Data from five rivers, including Oak Creek, Oregon (Milhous 1973), were used for the Parker et al. (1982) study. Equal mobility was found to accurately describe bedload transport in small to medium-sized, paved gravel-bed streams with steep or moderate slopes. Equal mobility failed to describe bedload containing throughput load (bedload with a sand content far in excess of the sand content in either the subpavement or pavement).

When equal mobility is truly present, all grain sizes on the bed are entrained at the same critical shear stress. Using the same Oak Creek data set that was used by Parker et al. (1982) to support equal mobility, Komar (1987) found critical shear stress to be an increasing function of grain size, but not as steep a function as described by the Shields curve (see Figure 2-1). The study done by Parker et al. (1982) used

only transport data taken when the discharge exceeded that which was necessary to break the pavement, but Komar (1987) included in his analysis data taken at lower discharges. Komar showed that the median grain size in a heterogeneous bed is entrained at roughly the same critical shear stress which would be necessary to entrain it from a homogeneous bed. Grain sizes coarser than the median size are entrained at lower shear stresses than if they were on a homogeneous bed, and finer sizes require a greater shear stress for entrainment than the shear stress found using the Shields curve. Komar suggested using the following relationship for the Shields' parameter of a particular size sediment in a mixture:

$$\theta_{ci} = a\left(\frac{D_i}{D_{50}}\right)^b, \tag{2.2}$$

where a and b are empirical coefficients, and i refers to the sediment size fraction represented by grain size D_i. Similar relationships were previously employed by Parker et al. (1982), Andrews (1983), and Church (1985). Komar proposed that selective entrainment is due to hiding and protrusion, as well as larger particles having smaller pivoting angles when present on a bed of smaller sizes (Li and Komar (1986); Komar and Li (1986)).

Data from some flume studies support equal mobility. In the case of a sediment feed flume in equilibrium, equal mobility must hold since the material fed into the flume must also pass out of the flume. Wilcock and Southard (1988) observed equal mobility in a sediment recirculating flume system, in which transport rates are determined solely by the the flow and bed sediment. In their flume experiments Wilcock and Southard (1988) used three different sediment distributions which had the same mean and distribution shape, but standard deviation varied. They also used data from other studies in which mixture sorting, grain shape, median grain size, and distribution of grain size all varied greatly. All of the transport data support equal mobility using the reference shear stress calculation criteria of Parker et al. (1982). Reference shear stress is defined as the shear stress necessary to produce a small reference transport rate. Reference shear stress is often used instead of critical shear

stress because its measurements are easier to obtain and more robust.

Other studies have tested whether equal mobility applies to the sand fraction of the bedload. To investigate this, Church et al. (1991) installed screened traps in the bed of a cobble gravel channel. The traps, which caught only the sediment up to about 10mm in size, were placed along a bar in the channel. Their data show that equal mobility of fine material only occurred in a limited range of grain sizes over a seasonal period. Equal mobility did not hold over short time scales. From visual observations it was concluded that the gravel began to move at discharges significantly higher than those required to move sand.

2.1.2 Sand and Gravel Mixtures

Although equal mobility is not a universally accepted phenomenon, a large number of studies have supported its existence, at least as a good approximation. Most of these studies have been on bed material with a unimodal and approximately log normal distribution (Kuhnle 1993). The distribution of bed sediment on many streams is not well represented by a log normal distribution, especially streams which contain both sand ($<$ 2mm) and gravel ($>$ 2mm). From a series of flume experiments on the incipient motion of sand and gravel mixtures, Kuhnle (1993) found that the presence of sand affected the transport of the gravel. In his experiments with a 100% sand mixture and a 100% gravel mixture, all sizes began to move at nearly the same bed shear stress. When sand and gravel were both present on the bed, all the sand sizes were still entrained at nearly the same bed shear stress. However, in the mixture, entrainment of the gravel sizes became a function of size (see Figure 2-3). For all of the experiments, the critical shear stress needed to entrain D_{50} was close to the value from the Shields curve.

A method for predicting transport rates in mixed gravel and sand bed rivers was developed by Wilcock (1997). From both field and flume experiments, Wilcock (1997) found that the sediment transport rates of sand and gravel need to be calculated separately because the sand and gravel fractions behave differently. Various regimes of transport exist depending on the percentage of sand on the bed. When the bed

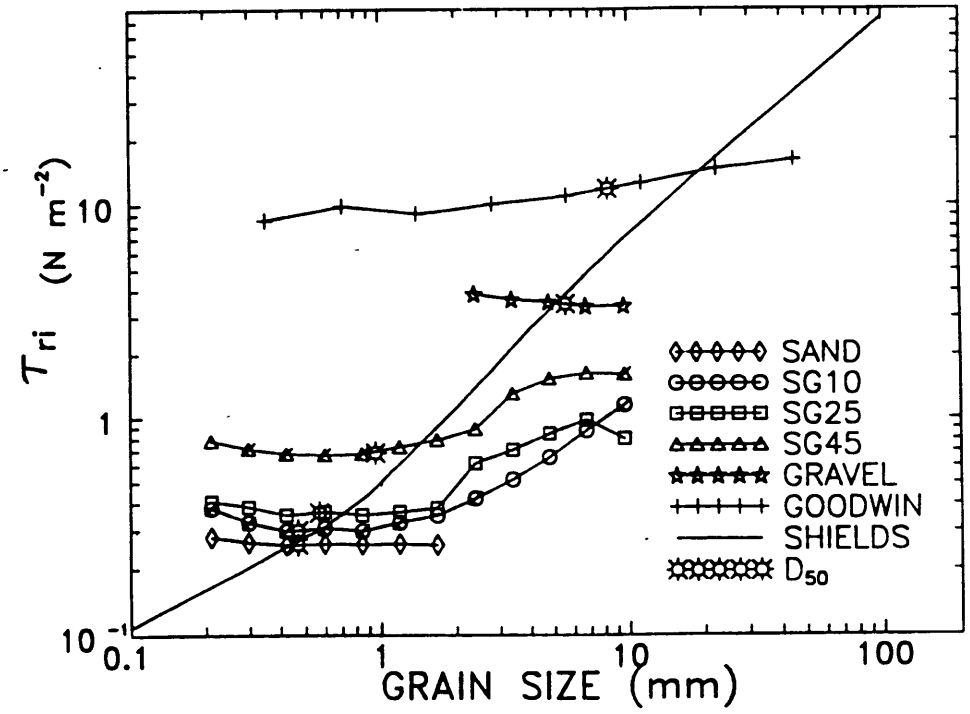

Figure 2-3: Reference shear stress versus grain size from Kuhnle (1993). The mixtures labeled sand and gravel gravel are mixtures containing only sand and gravel sizes respectively. The mixtures labeled SG10, SG25 and SG45 contain 10%, 25%, and 45% gravel respectively. The mixture labeled Goodwin is from Goodwin Creek, which is a gravel-bed channel with bi-modal distribution of bed material.

contains less than 10% sand, the effects of the absolute size of the grains seem to be balanced by the relative size of the grains and all sizes move at approximately the same rate when scaled to their proportion in the bed. For sand contents between 10% and 30%, sand fills the pores between the gravel grains and collects in patches. Sand will begin to move at lower flows than the gravel and will have a higher transport rate for a given flow. When the sand content of the bed reaches the 30% to 50% range, the bed makes the transition from framework-supported to matrix-supported. This implies that the proportion of finer (matrix) material is large enough to reduce the amount of contact between the coarser (framework) particles to almost zero, making the coarser particles easier to entrain. Because the finer particles arrange themselves in patches, sand transport rates are similar to those for unisize sand. When the sand content is greater than 50%, the bed is fully matrix-supported. Sand is transported as though the bed were homogeneous. Gravel is transported at flows smaller than those needed to initiate motion of unisize gravel because of the presence of the sand.

Using various data sets, Wilcock (1997) finds the Parker (1979) transport function (a power approximation of the Einstein (1950) bedload curve) to best approximate the measured gravel transport rates. The Parker/Einstein transport function was altered to correctly predict sand transport rates. The gravel and sand transport equations are:

$$Q_s^g = \frac{11.2\rho_s f_g}{(s-1)g}\left(\frac{\tau}{\rho}\right)^{1.5}\left[1-\frac{\tau_{cg}}{\tau}\right]^{4.5} \quad \text{and} \tag{2.3}$$

$$Q_s^s = \frac{11.2\rho_s f_s}{(s-1)g}\left(\frac{\tau}{\rho}\right)^{1.5}\left[1-\sqrt{\frac{\tau_{cs}}{\tau}}\right]^{4.5}, \tag{2.4}$$

where Q_s^g and Q_s^s are the transport rates of gravel and sand, respectively, here in units of kg/ms; f_g and f_s are the proportion of gravel and sand on the bed, respectively; $s = \rho_s/\rho$; and τ_{cg} and τ_{cs} are the critical shear stress values to entrain the gravel and sand portions, respectively. The representative gravel and sand sizes are the gravel and sand modes, D_g and D_s, respectively.

Wilcock (1997) developed two graphs for determining critical shear stress (Figure 2-4). The figure shows plots of dimensionless reference shear stress, $\tau_r^* = \frac{\tau_r}{(\rho_s-\rho)gD}$,

for both sand and gravel as a function of proportion sand on the bed. Critical shear stress is easily determined from reference shear stress using the relation $\tau_c = \xi\tau_r$ where $\xi < 1$. The reference shear stress values used in Figure 2-4 were obtained by plotting transport data as a function of shear stress. Some extrapolation was necessary for smaller sizes. Reference shear stress varies with grain size and percentage of sand on the bed. The effects of grain size are included in τ_r^*. The figure suggests that τ_{rg}^* approaches a value of approximately 0.04 for small sand contents (less than 10%) and approximately 0.01 for large sand contents (greater than 40%). In the range between these two limits, the reference shear stress for gravel decreases as the percentage of sand on the bed increases. The variation of τ_{rs}^* is similar to that of τ_{rg}^*. When sand percentage is high, τ_{rs}^* is approximately 0.04. A dimensionless reference shear stress value of 0.04 is the conventional value for narrowly sorted sediment (Wilcock 1997). In the range of sand percentage between 10% and 40%, τ_{rs}^* decreases as the percentage of sand on the bed increases. When the percentage of sand on the bed is small (<10%) sand tends to get trapped in the gravel pores, making sand harder to entrain than if it were on a homogeneous bed and gravel easier to entrain than if it were on a homogeneous bed. Because of this phenomenon, $\tau_{rs} \approx \tau_{rg}$ when f_s is small.

The sediment transport equations and reference shear stress plots developed by Wilcock (1997) are used in this study. The next chapter will discuss their application. Wilcock's method for determining sediment transport in a sand and gravel mixture was chosen because it is general and well formulated. Also, it uses two grain sizes to represent a distribution, which is very desirable for modeling purposes, since it reduces the number of computations.

(a)

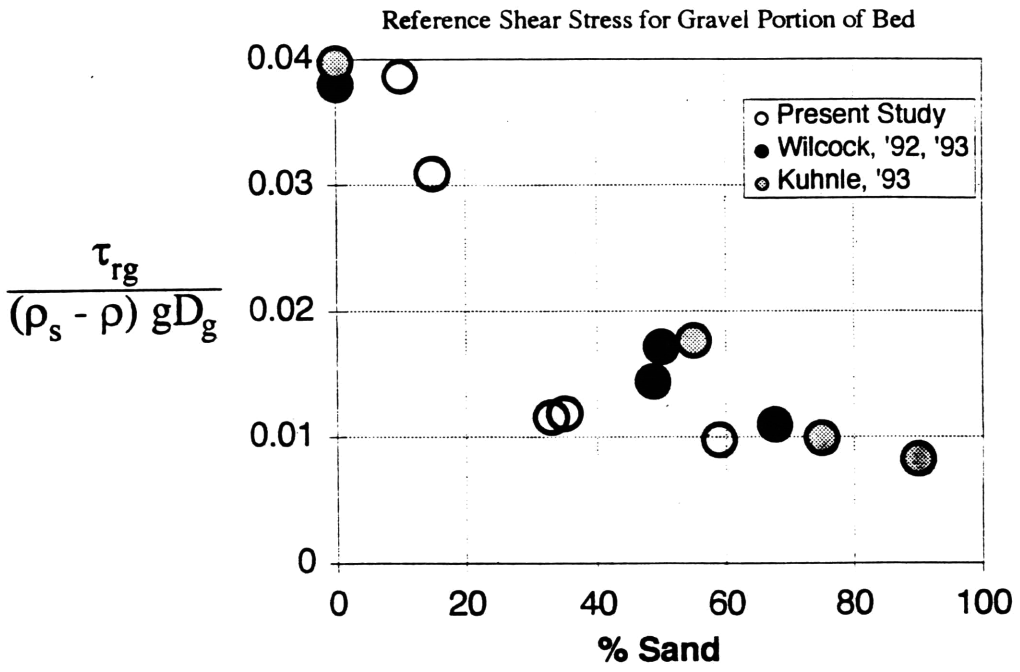

(b)

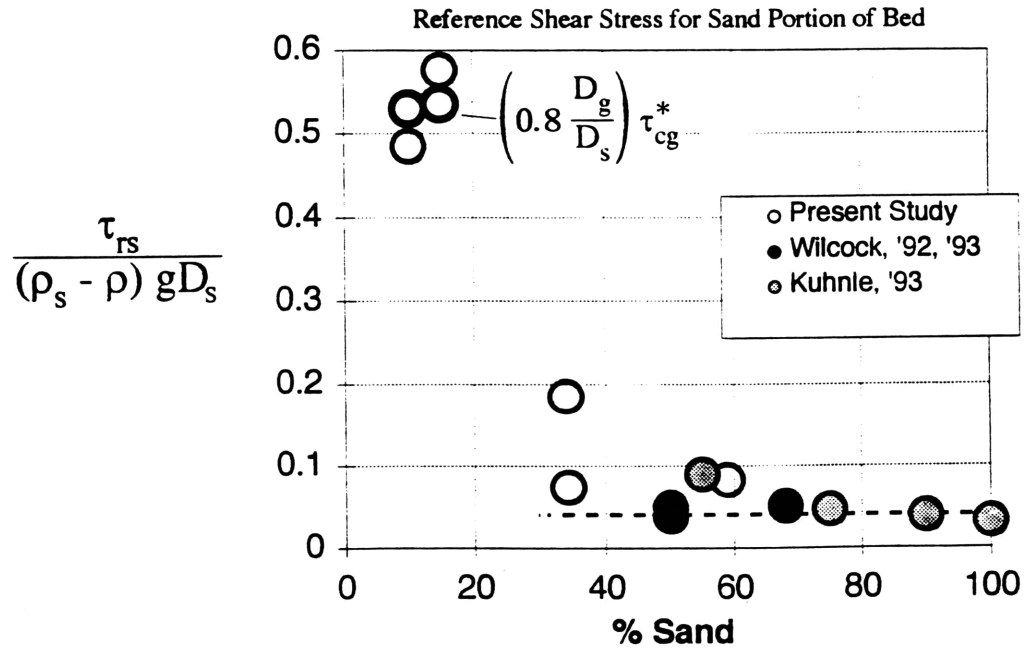

Figure 2-4: (a) and (b) show dimensionless reference shear stress for gravel and sand, respectively, as a function of sand content on the bed (from Wilcock (1997)).

Chapter 3

Model Description

The numerical model used for this study is a revised version of GOLEM, a previously developed landscape evolution model (Tucker 1996). The model represents the topographic surface with a rectangular grid of cells of the same size. Tectonic uplift, hillslope processes, and fluvial erosion act on each cell, evolving the topography through time. For this study, GOLEM was modified to allow for sediment with two grain sizes (sand and gravel). A layering scheme was developed to track the texture of deposited layers and to allow for more realistic conditions during erosion. A thorough description of GOLEM is given in Tucker (1996). A short overview of the model is given here, focusing on the additions made for this work.

3.1 Model Algorithms and Equations

3.1.1 Drainage Network

As precipitation falls on a landscape, the slope of the topography dictates the direction of water flow and produces a network of channels. In the model, water is assumed to flow from a grid cell in the direction of steepest decent towards one of the surrounding eight cells (Figure 3-1). If a cell has no lowest neighbors, GOLEM has a complex algorithm to account for ponding and overflow from a closed topographic depression. The ponding algorithm was used in all of the model runs in this study.

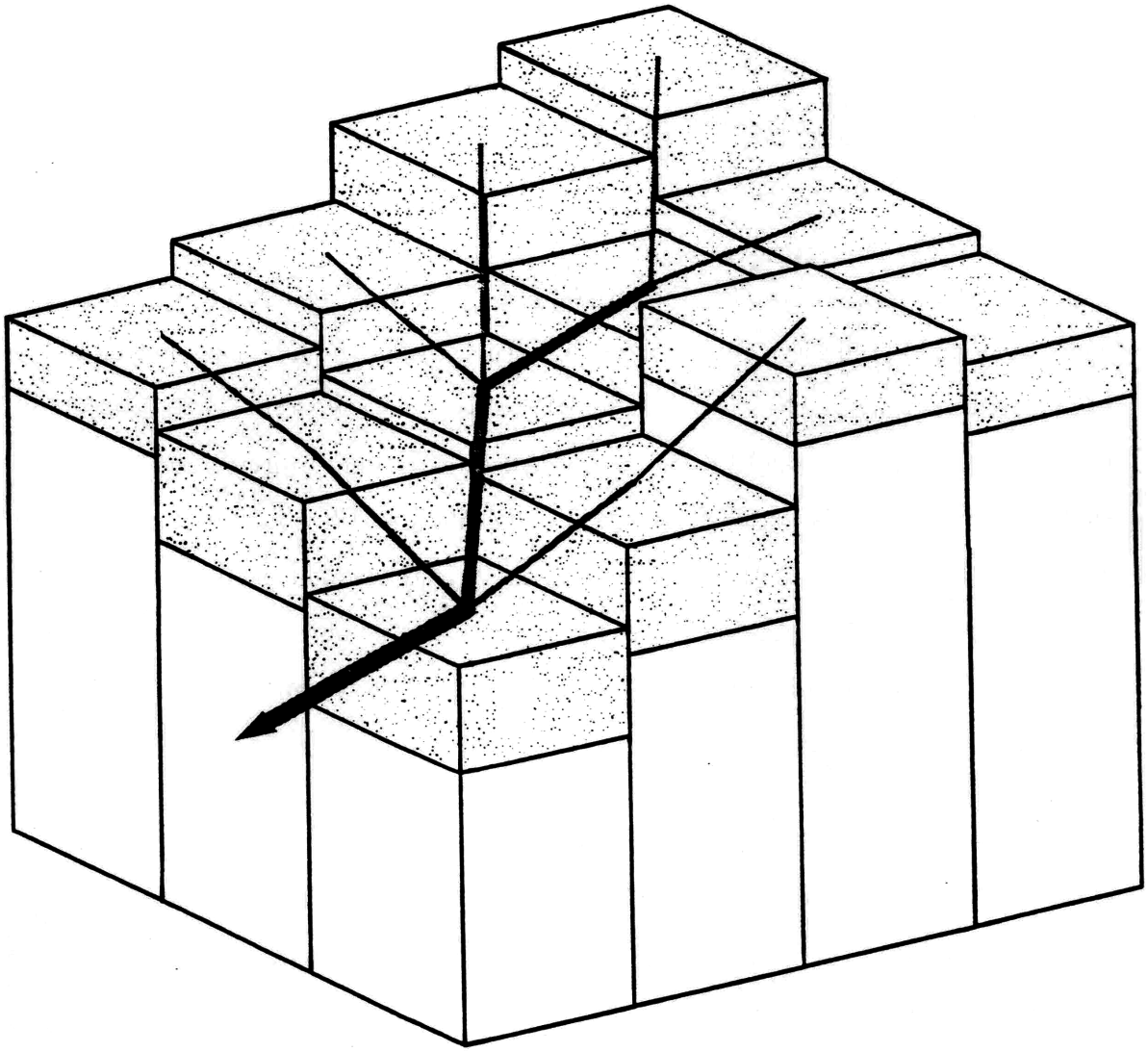

Figure 3-1: Model representation of topography as a grid of cells, with water and sediment cascading down the grid along the route of steepest descent, taken from Tucker (1996).

3.1.2 Fluvial Erosion

The bedload transport equations developed by Wilcock (1997) are used in this study (see section 2.1.2). Equations 2.3 and 2.4 are recast below as volumetric load per time.

$$Q_s^g = \frac{11.2 W f_g}{(s-1)g}\left(\frac{\tau}{\rho}\right)^{1.5}\left[1-\frac{\tau_{cg}}{\tau}\right]^{4.5} \tag{3.1}$$

$$Q_s^s = \frac{11.2 W f_s}{(s-1)g}\left(\frac{\tau}{\rho}\right)^{1.5}\left[1-\sqrt{\frac{\tau_{cs}}{\tau}}\right]^{4.5} \tag{3.2}$$

The following relationships were assumed in order to calculate sediment transport rates:

$$W = k_1 Q^{0.5} \tag{3.3}$$

$$Q = PA \tag{3.4}$$

$$Q = VWd \tag{3.5}$$

$$V = n^{-1} R^{2/3} S^{1/2} \tag{3.6}$$

$$R \approx d \tag{3.7}$$

$$\tau = \rho g R S \tag{3.8}$$

in which W is channel width; k_1 is a parameter; Q is water discharge; P is effective precipitation; A is drainage area; V is cross-section averaged water velocity; d is water depth; n is Manning's roughness coefficient; R is hydraulic radius and S is local slope. Equation 3.3 comes from the downstream hydraulic geometry equations of Leopold and Maddock (1953). In hydraulic geometry studies the exponents and not the coefficients are studied, because the exponents are general whereas the coefficients change from river to river. In those studies which give a value of k_1 (e.g. Wolman (1955)) it is $\sim O(10^0)\frac{\text{sec}^{0.5}}{\text{m}^{0.5}}$, so k_1 was chosen to be 1.0. Equation 3.4 is a simple representation of discharge where P is that part of the rainfall which goes into surface runoff. Here P is assumed to be constant across the entire basin. Equation 3.5 comes from continuity of mass. Mean velocity (in metric units) is calculated using the

formula of Robert Manning (equation 3.6). A value of 0.03 was used for n, which represents a clean, straight, fullstage, natural stream with no rifts or deep pools (taken from table 5-6 in Chow (1959)). The assumption made with equation 3.7 is appropriate for channels in which $W \gg d$. Equation 3.8 holds for steady, uniform flow.

Substituting equations 3.3 - 3.8 into equations 3.1 and 3.2 gives the following equations for sediment transport:

$$Q_s^g = k_2 f_g A^{0.95} S^{1.05} \left[1 - \frac{\tau_{cg}}{\rho g} n^{-0.6} (PA)^{-0.3} S^{-0.7}\right]^{4.5} \quad \text{and} \tag{3.9}$$

$$Q_s^s = k_2 f_s A^{0.95} S^{1.05} \left[1 - \frac{\tau_{cs}^{0.5}}{(\rho g)^{0.5}} n^{-0.3} (PA)^{-0.15} S^{-0.35}\right]^{4.5} , \tag{3.10}$$

where

$$k_2 = \frac{11.2 P^{0.95} g^{0.5} n^{0.9}}{(s-1)g} . \tag{3.11}$$

Calculation of τ_{cg} and τ_{cs} is done by approximating curves to Figures 2-4 (a) and (b). When the bed contains more than 40% sand, the dimensionless reference shear stress for both gravel and sand are constant at 0.01 and 0.04, respectively. A linear fit was made for both τ_{rg}^* and τ_{rs}^* in the region where the percentage of sand on the bed is between 10% and 40%. When the bed contains less than 10% sand, both τ_{rg}^* and τ_{rs}^* are constant again, but the value of τ_{rs}^* depends on the grain sizes present on the bed. The relation $\tau_{rs}^* = \left(0.8\frac{D_g}{D_s}\right)\tau_{rg}^*$ is used when there is less than 10% sand on the bed. τ_{rg}^* has a constant value of 0.04. The relation $\tau_c = 0.8531\tau_r$ (Wilcock 1997) is used to convert reference shear stress to critical shear stress for both sand and gravel.

Equations 3.9 and 3.10 are used for calculating sediment transport rates of gravel and sand individually. Although a number of simplifications were made to develop these equations, the coefficients still contain constants with actual units. This was done so that the model time-step could be as realistic as possible.

For the purposes of this study, the landscape is assumed to be transport-limited. Transport-limited erosion describes a channel which has enough sediment on the bed

to provide the flow with the maximum amount of material it can transport. In real fluvial systems the channel may not be covered with sediment in all areas, in which case bedrock erosion might occur. In this study the sediment supply is unlimited. The purpose of this study is to examine the effects of grain size interactions in a fluvial system. Although unlimited sediment supply may be an unrealistic assumption in some cases, this simpler problem still proves to have many interesting and realistic results.

The rate of erosion in the transport-limited case is calculated as

$$\frac{\partial z}{\partial t} = \frac{\sum_{i=1}^{n} Q_{si}^{in} - \sum_{i=1}^{n} Q_{si}^{out}}{a} \tag{3.12}$$

where z is the total bed elevation; t is time; $\sum_{i=1}^{n} Q_{si}^{in}$ is the sum of the sediment transport rates of each size fraction coming into the current grid cell; $\sum_{i=1}^{n} Q_{si}^{out}$ is the sum of the sediment transport rates of each size fraction calculated at the current grid cell; and a is the grid cell area, which remains constant. For this study of sand and gravel mixtures, $n = 2$.

3.1.3 Hillslope Processes

Slope-dependent processes such as soil creep and rain splash are modeled using a linear diffusion equation. Sediment transport by diffusive processes is described by the equation

$$q_{di} = k_d f_i \nabla z, \tag{3.13}$$

where q_{di} is the volumetric transport rate per unit slope width (in this case, cell width) of size fraction i. Diffusion does not contribute to sorting of grains because the diffusion rate of each grain size is proportional to its percentage in the active layer.

3.1.4 Layering Algorithm

An algorithm to create and destroy layers of sediment was developed. During fluctuations between erosion and deposition in a fluvial system, the erosion rates depend on the texture of material previously deposited. The algorithm insures proper calculation of erosion rates and allows the user to track the texture of alluvial sedimentary deposits.

The active layer is that part of the bed in which particles are subject to entrainment through contact with the near-bed water flow (Rahuel et al. 1989). Active layers have been incorporated in various ways into a number of channel models (e.g., Borah et al. (1982b), Park and Jain (1987), Rahuel et al. (1989), and van Niekerk et al. (1992)). In previous models the active layer has been modeled as either a single surface layer or multiple surface layers in which sediment is exchanged with the flow. Below the surface layer(s) is a layer of parent material of constant texture which supplies the surface layer(s) with sediment. Material can only be eroded from the active layer. In previous modeling efforts more sedimentary layers could not be created. When deposition occurred, material would be transferred from the active layer to the parent material and stored as the texture of the parent material, regardless of its original texture.

Theoretically, the active layer depth depends on the distribution of grain-sizes on the surface of the bed. In numerical models, the depth of the active layer also depends on the time-step. The longer the time-step, the deeper the active layer needs to be if the system is erosional. The layering algorithm in this model also uses an active layer of constant depth. The active layer depth is not calculated from a formula; it is chosen by considering other parameter values in the model, including the time-step and the magnitude of precipitation.

The surface active layer depth may change during a single time-step, but at the end of a time-step, it always returns to its original depth at every grid cell. The bottom layer of sediment (the substrate or parent material) is essentially infinitely deep so that if erosion takes place there is always enough material to replenish the

active layer. The texture of the substrate at every grid cell in the basin is the same. Every layer of sediment is assumed to be well-mixed.

The layering method is broken into three parts: total erosion, total deposition, and both erosion and deposition. Both erosion and deposition can occur in single time-step because sediment transport rates are calculated separately for each grain size.

3.1.4.1 Erosion

Erosion occurs when the amount of material in the sediment load coming into a grid cell is less than the amount of material which can be carried out of the grid cell. The amount of erosion of a single grain size is limited by the supply of that grain size in the active layer. If the calculated total amount of erosion is larger than the active layer depth, the time step is decreased, unless the time-step has already reached its minimum value. The time-step is also decreased when the total erosion exceeds a given percentage of the elevation difference between the current grid cell and its lowest neighbor (described in detail in Tucker (1996)). Once the minimum time-step is reached, erosion is limited to only the material which is in the active layer. When the landscape reaches dynamic equilibrium, the amount of material eroded at each grid cell is always less than the depth of the active layer.

Figure 3-2 illustrates an example of erosion of both grain sizes. In Figure 3-2 (a), the amount of material to be eroded has been calculated and the algorithm has checked to see that the material is available from the active layer. In Figure 3-2 (b), the material is eroded from the active layer and added to the sediment load to be carried to the next node. The active layer depth is depleted. In Figure 3-2 (c), the active layer is refilled to its original depth with material of the same texture as that of the layer below. The layer below then decreases in size, but its texture remains the same. If there is not enough material in the layer below the active layer, the layer below the active layer is removed and all of the material from this layer replenishes the active layer. The active layer is further replenished with material from the next lower layer, until the active layer returns to its proper depth. The texture of the

active layer can change during the process of removing material through erosion and adding material from the layer(s) below.

3.1.4.2 Deposition

Deposition occurs when the amount of material in the sediment load coming into a grid cell is greater than the amount of material which can be carried out of the grid cell. Deposition of both grain sizes is illustrated in Figure 3-3. Figure 3-3 (a) shows the total amount of material which will be deposited into the active layer. In Figure 3-3 (b), material of the depth to be deposited and the texture of the active layer is moved from the active layer into the layer below. This is done before any material is deposited into the active layer. Figure 3-3 (c) shows the active layer after it is replenished with the deposited material. The active layer depth is returned to its initial depth, and has a new texture that reflects the admixture of the new material. The layer below grows and probably also changes texture.

All of the layers below the active layer (except for the substrate which will never have material deposited into it) have a maximum depth. Before material is deposited into a layer below the active layer, the depth of the layer is checked. If the layer depth will surpass the maximum layer depth (a model parameter) once material is deposited into it, a new layer is created between this layer and the active layer. The new layer is made up of the material which needs to be moved out of the active layer. The depth and texture of the layer which was previously below the active layer are stored.

3.1.4.3 Simultaneous Deposition and Erosion

It is possible for one size fraction of material to be eroded and the other to be deposited. If this is the case, the active layer depth may increase or decrease. If there is net erosion, material is simultaneously eroded and deposited and then the active layer is updated with material from below as was described in section 3.1.4.1. If there is net deposition, material is simultaneously eroded and deposited and then material is moved below as was described in section 3.1.4.2. In the case of net deposition, some

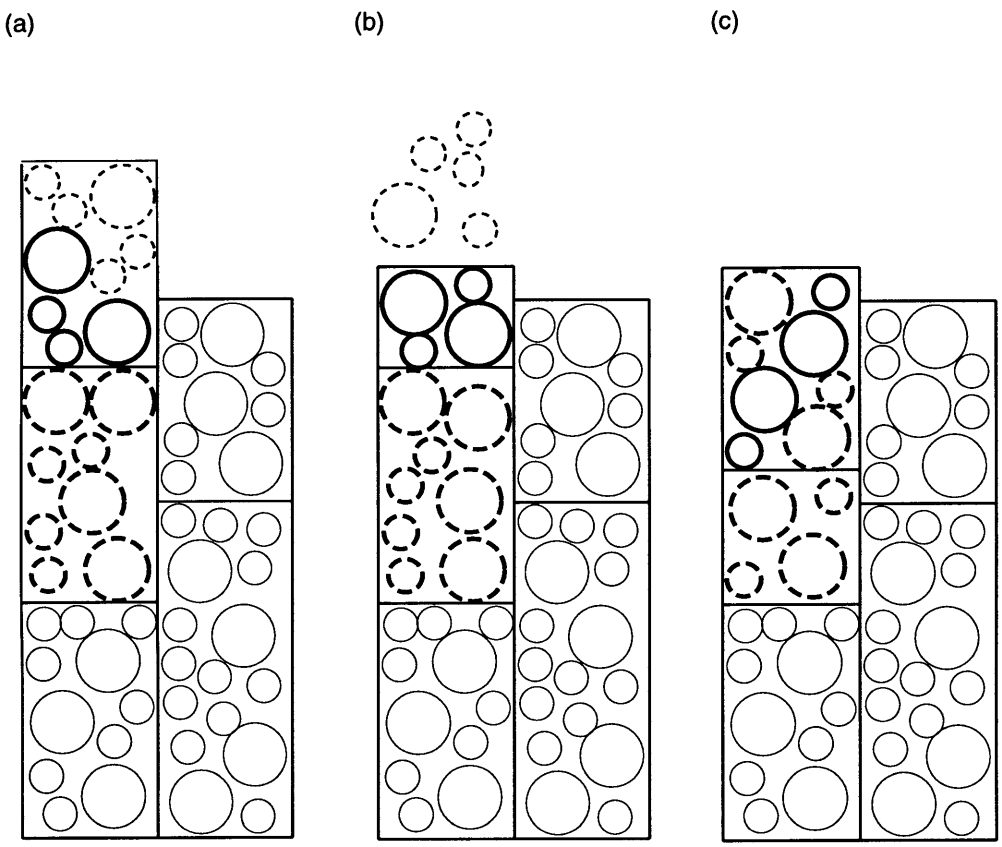

Figure 3-2: Cartoon example of erosion at a single grid cell. First the amount of material to be eroded (drawn with the thin dashed line) is calculated, shown in (a). In (b), the material is eroded away and becomes part of the sediment load. The active layer is depleted. Finally, in (c) the active layer is replenished with material from the layer below, drawn with a thick dashed line.

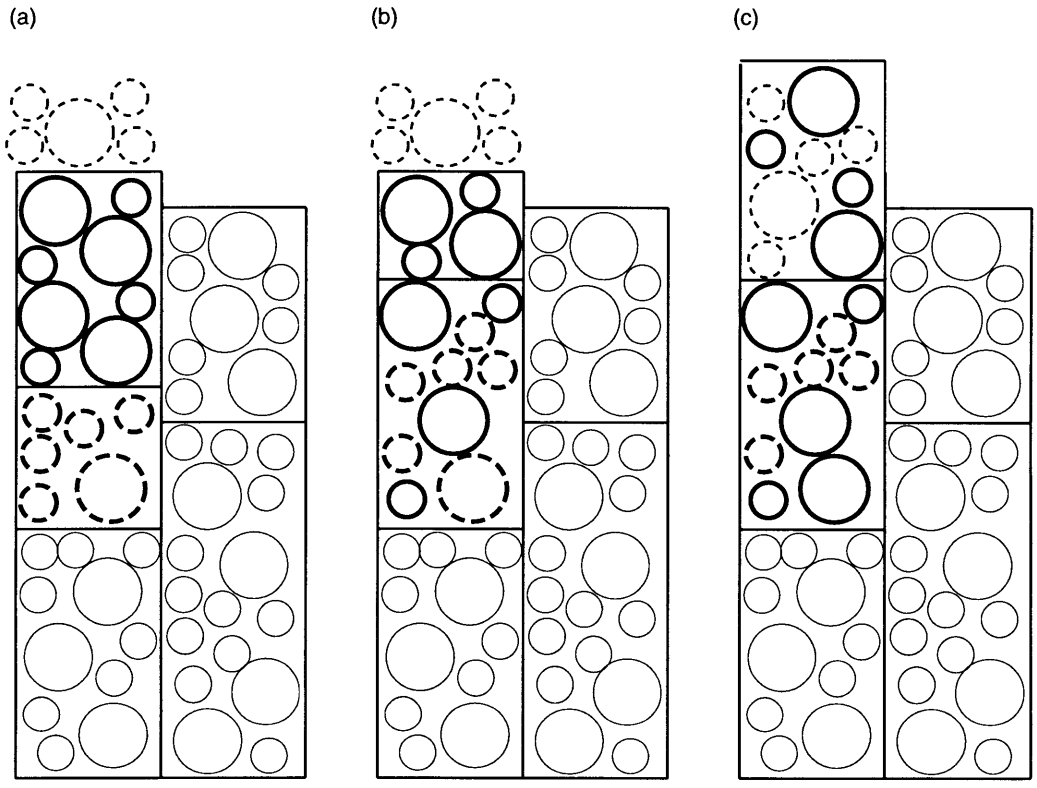

Figure 3-3: Cartoon example of deposition. (a) shows the initial condition before any changes have been made to the layers. The depth of deposited material has been calculated. The material to be deposited, shown with thin dashed lines, is not yet part of a layer. In (b) material has been moved out of the active layer to make room for the new material to be deposited. The active layer is replenished with the deposited material in (c).

of the material which was just deposited may be moved into lower layers. Given the fact that simultaneous erosion and deposition is not the norm, and that the texture of the active layer is only slightly changed, this method is adequate.

Chapter 4

Single Grain Size Modeling Study

The sensitivity of the model to changes in a single effective grain size is discussed in this chapter. In dynamic equilibrium, concavity in the modeled basins increases with effective grain size. Realistic concavities are only produced with effective grain sizes in the gravel range. It is hypothesized that the difference in concavity results between modeled and real basins may be a result of sediment heterogeneity and sorting.

4.1 Varying Effective Grain Size

Five basins with effective grain sizes of 0.5mm, 1mm, 8mm, 16mm, and 50mm were evolved to dynamic equilibrium. For the two basins with an effective grain size in the sand range (< 2mm), equation 3.10 was used to calculate sediment transport. Equation 3.9 was used to calculate sediment transport in the basins with an effective grain size in the gravel range (> 2mm). A dimensionless reference shear stress value of 0.04 was used for both gravel and sand. This value is appropriate for homogeneous beds (see Figure 2-4).

The initial surface used for all of the runs was flat with a small amount of roughness. The uplift rate across the entire basin was constant. The outlet drained to a cell with constant elevation. This outlet was the only location in which water and sediment could leave the system. Table 4.1 shows the parameter values and domain information used for the experiments in this chapter and the next. The parameter

Parameter	Value
Uplift Rate	10^{-4}m/yr
Diffusivity Coefficient	10^{-1}m^2/yr
Effective Precipitation Rate	0.3m/yr
Pixel Size	1600m^2
Grid Size	$48x48$ cells^2
Time Step	10 years

Table 4.1: Table of parameter values and domain information used in experiments with a constant precipitation.

values remained constant for the entire duration of each model run.

4.2 Basin Concavity

The critical shear stress for entrainment controls basin concavity in dynamic equilibrium. Drainage basins which are composed of sediment with a single effective grain size have a single critical shear stress for entrainment of particles throughout the entire drainage basin. Therefore, since critical shear stress varies directly with grain size in homogeneous sediment, basin concavity also varies directly with grain size in basins composed of homogeneous sediment. This result is illustrated in both the analytical solution of the bedload transport equation in dynamic equilibrium and also in the numerical modeling results.

In dynamic equilibrium, drainage basin concavity can be found from the sediment transport equations. A basin reaches dynamic equilibrium when the rate of addition of material to the system (e.g., through tectonic uplift) equals the erosion rate. In the model, material is added to the system through uplift. In dynamic equilibrium, the sediment transport rate at any grid cell must be equal to the amount of material added to the system upstream of the cell. This is expressed in the following equation:

$$UA = Q_s, \tag{4.1}$$

where U represents uplift rate (isovolumetric conversion of rock to sediment is im-

plied). Substituting an equation for sediment transport into equation 4.1 and rearranging, one obtains the following relationship,

$$S \propto A^{\eta} \tag{4.2}$$

where η is an index of the stream-profile concavity (also referred to here as basin concavity).

Tucker and Bras (1997) examined the trend in concavity with increasing erosion threshold. Using a sediment transport equation of the form

$$Q_s = k(A^m S^n - \phi)^{\gamma} \tag{4.3}$$

where k, m, n, and γ are constants and ϕ is an erosion threshold (e.g., critical shear stress), they found that the relation between local slope and contributing area depends on the degree to which the threshold term dominates. Substituting equation 4.3 into equation 4.1 and rearranging, the expression for local slope in equilibrium conditions is

$$S = \left(A^{\left(\frac{1}{\gamma} - m\right)} \left(\frac{U}{k}\right)^{\frac{1}{\gamma}} + \phi A^{-m} \right)^{\frac{1}{n}}. \tag{4.4}$$

If the threshold term is small

$$S \propto A^{\left(\frac{1}{\gamma} - m\right)^{\frac{1}{n}}}; \tag{4.5}$$

however if the threshold term dominates

$$S \propto A^{\frac{-m}{n}}. \tag{4.6}$$

Since γ, m, and n are all positive values and $\gamma > 1$, this implies that as the threshold term dominates, slope becomes more dependent on contributing area, or in other words, the stream-profile becomes more concave.

Although the sediment transport equations used to evolve the basins in this study are not the same as the equation used by Tucker and Bras (1997), the equations have a similar form. Substituting equations 3.9 and 3.10 into equation 4.1 for the sediment

Effective Grain Size	0.0005m	0.001m	0.008m	0.016m	0.05m
Slope of Slope-Area Plot	-0.14	-0.18	-0.31	-0.34	-0.37

Table 4.2: Table of concavity results for basins with a single effective grain size.

transport rate, and assuming $\tau_c = 0$, the analytical solution for η is 0.048. A positive value of η implies a convex profile which does not make sense for a stream-profile. However, when $\tau_c = 0$, the analysis of Tucker and Bras (1997) suggests that stream-profile concavity is at its smallest value. As τ_c increases, or equivalently effective grain size increases, the stream-profile should become more concave.

The numerical results illustrate the increase in concavity with effective grain size. The topography of three of the five basins which were evolved to dynamic equilibrium is shown in Figure 4-1. Plots of local slope versus drainage area are shown in Figure 4-2. Table 4.2 shows the values of η for all five of the simulated basins. The basin with the smallest grain size, and therefore smallest critical shear stress, has a concavity closest to that of a basin with $\tau_c = 0$.

There is no universal observed value for stream-profile concavity. Using data from 11 drainage basins in the Appalachian Plateau, Flint (1974) found that η ranged between -0.37 to -0.827 with an average value of -0.60. Tarboton et al. (1989) analyzed 21 different basins from across the United States and found η varied between -0.25 and -0.85. The range in observed values of η is quite large, however, in the two simulated basins with effective grain sizes of 0.0005m and 0.001m, the value of η doesn't fall in the observed range.

4.3 Discussion

The sensitivity of the model to changes in a single effective grain size was examined in this chapter. Basin concavity was found to increase with effective grain size. Realistic concavities were not produced if the effective grain size was in the sand size range, but reasonable basin concavities were produced when the sediment had an effective grain size in the gravel range.

(a)

0.0005m Effective Grain Size

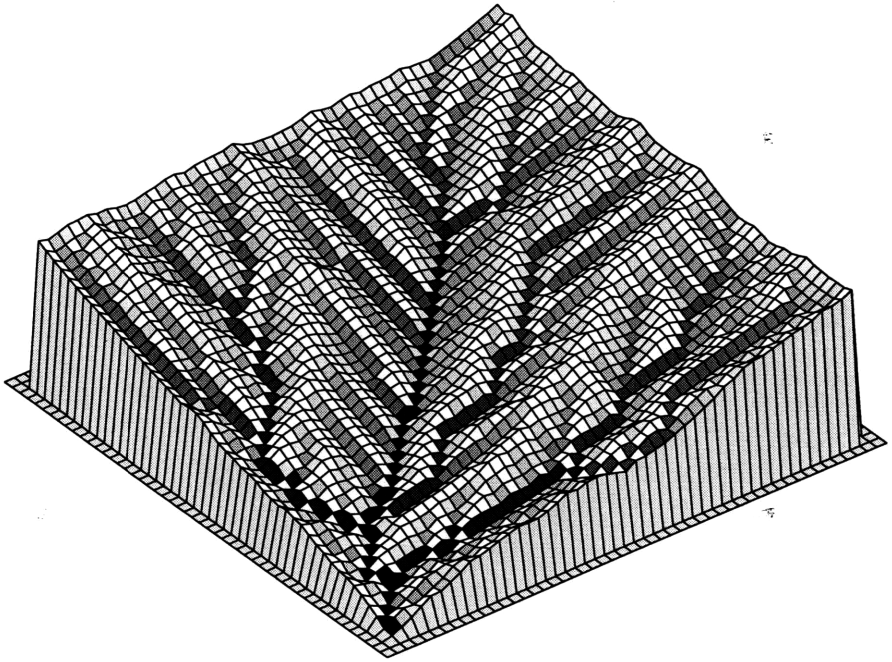

(b)

0.008m Effective Grain Size

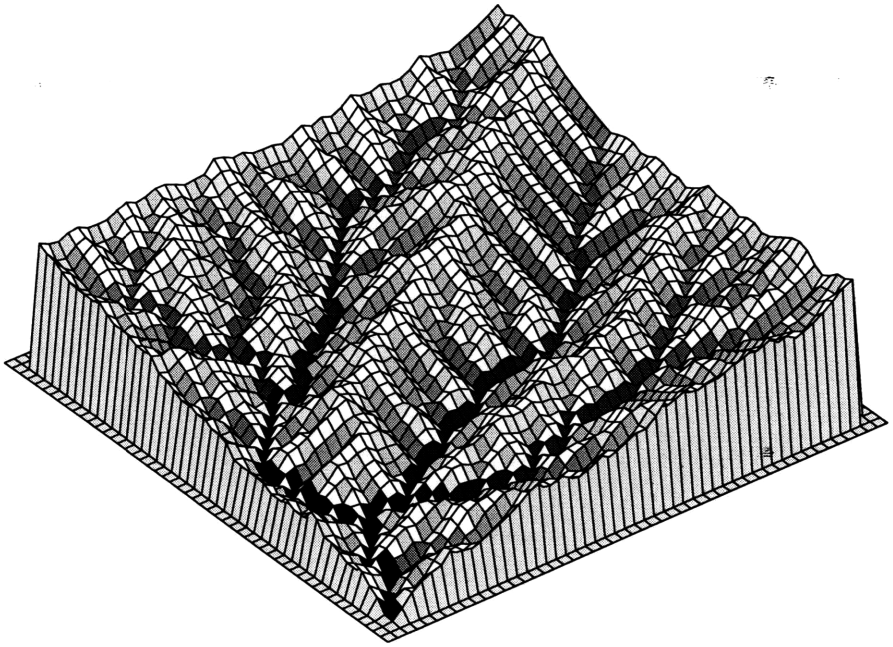

(c)

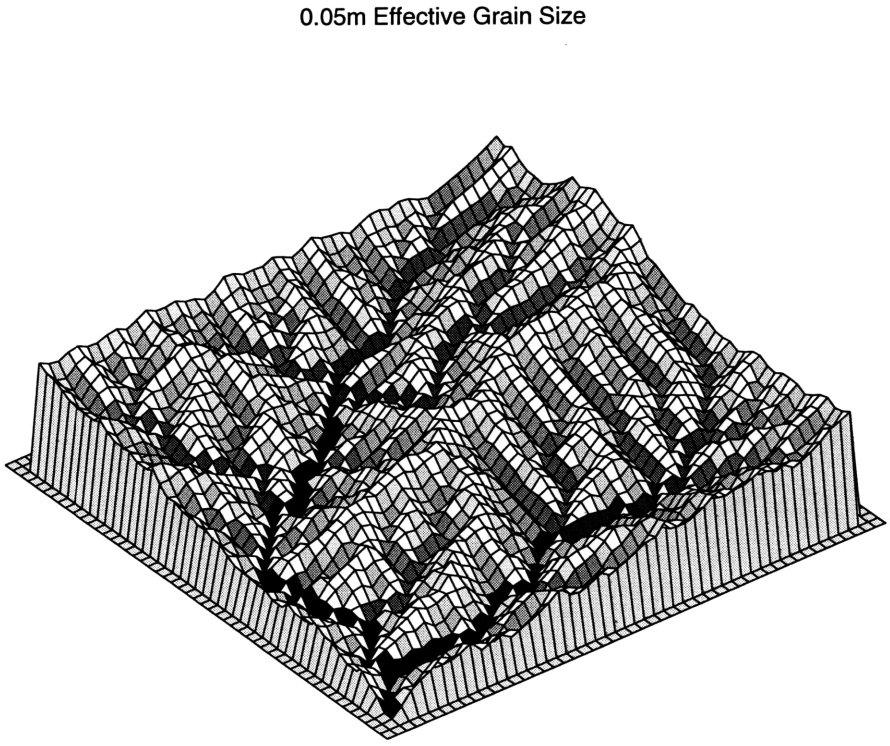

Figure 4-1: Topography for three basins composed of homogeneous sediment with different effective grain sizes. Each node is shaded according to its drainage area.

(a)

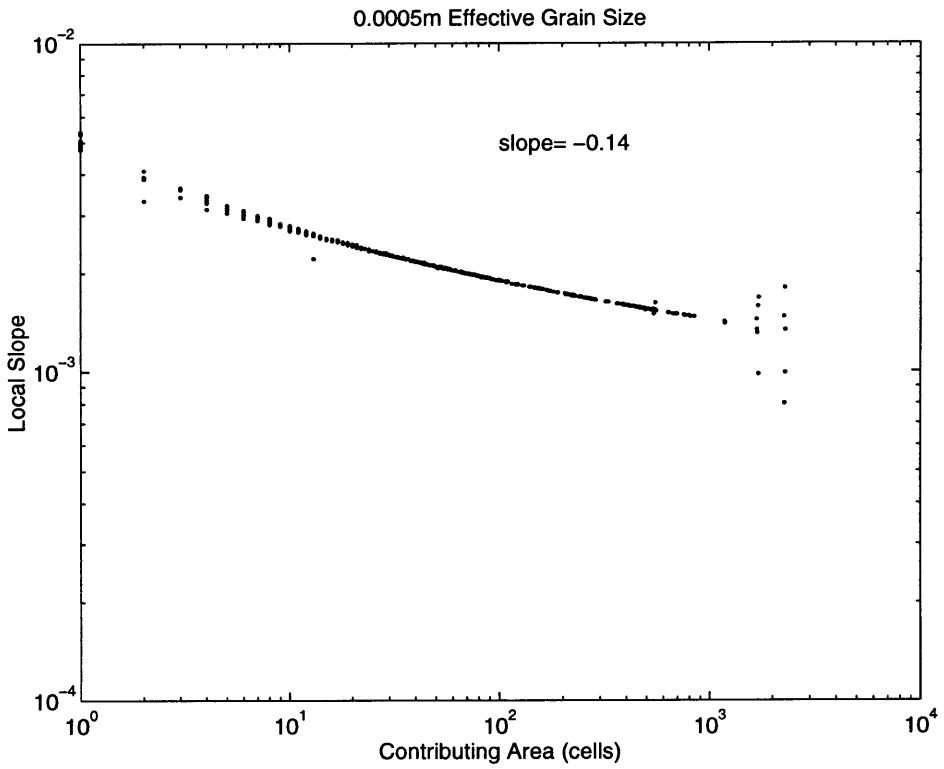
0.0005m Effective Grain Size
slope= −0.14
Local Slope
Contributing Area (cells)
10^{-2}
10^{-3}
10^{-4}
10^{0}
10^{1}
10^{2}
10^{3}
10^{4}

(b)

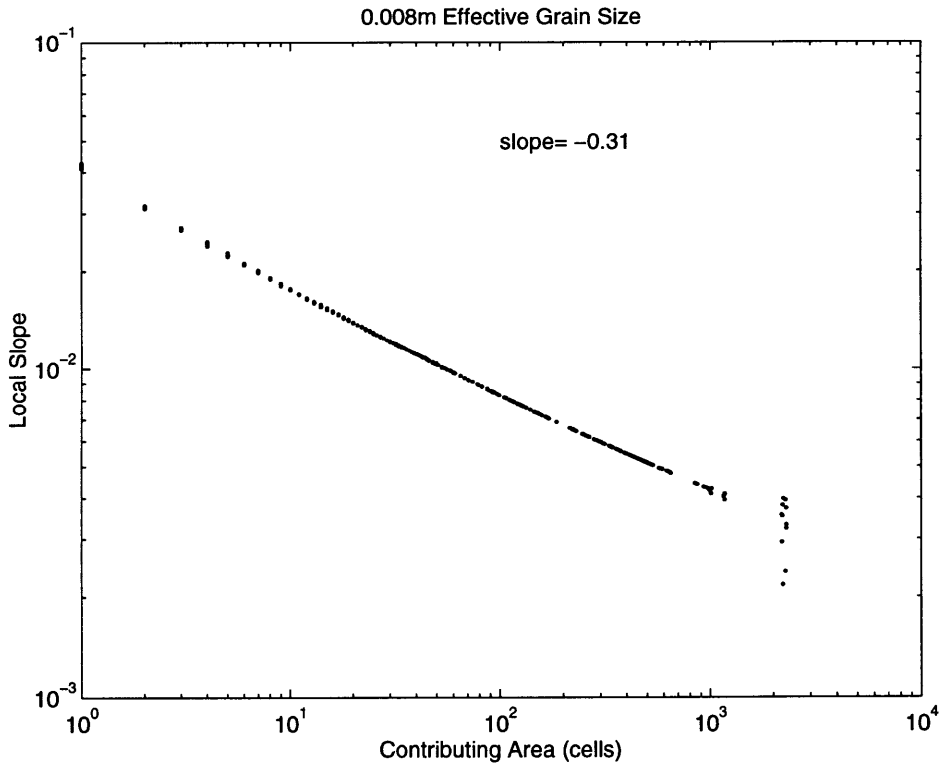
0.008m Effective Grain Size
slope= −0.31
Local Slope
Contributing Area (cells)
10^{-1}
10^{-2}
10^{-3}
10^{0}
10^{1}
10^{2}
10^{3}
10^{4}

(c)

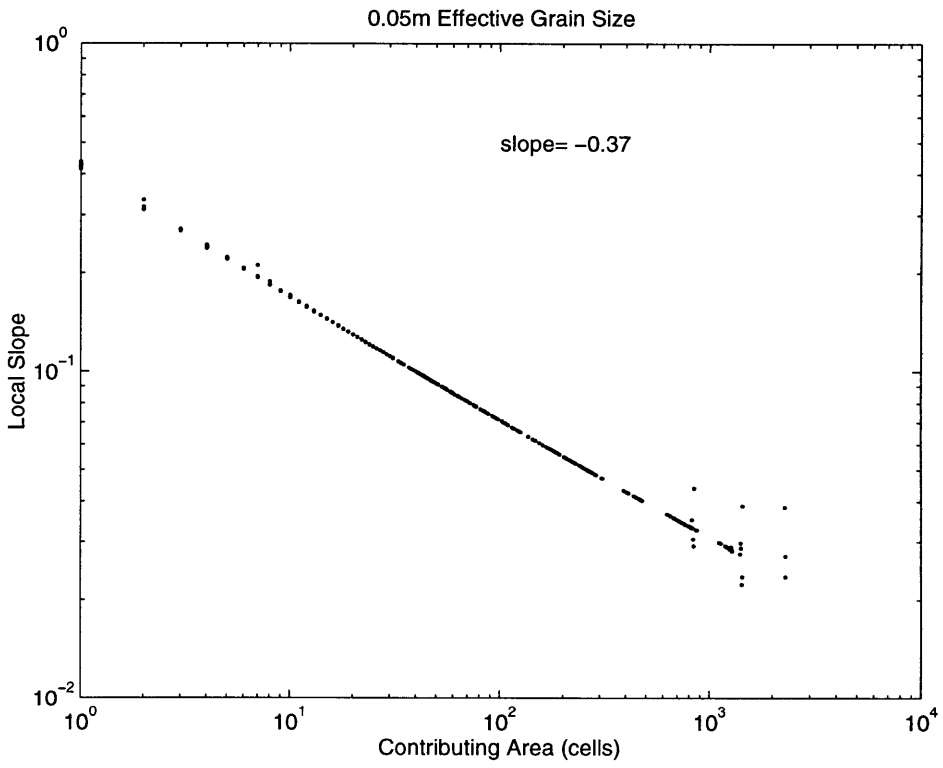

Figure 4-2: Slope-area plots for three basins composed of homogeneous sediment with different effective grain sizes. The value of slope given is from a linear fit to the data for drainage areas between 10 and 1000 pixels.

Basin concavity is controlled by the bedload transport and velocity equations. An error in these equations could lead to unreasonable morphologies. Although numerous bedload equations exist, they all produce an unrealistically small basin concavity when critical shear stress is small. The assumption that all sediment is moving as bedload may be the source of the error, not the form of the bedload equations. Suspended sediment is most of the sediment load in a sand-bed reach, so to ignore it may be leaving out an integral part of the system. The addition of suspended sediment transport may lead to more realistic basin concavities.

Although the lack of suspended sediment may be linked to the concavity results, it is hypothesized that this is not the main reason for the unrealistic morphologies in the finer basins. Using a single effective grain size can not capture the interactions between sediment grains of various sizes. It is hypothesized that these interactions are essential to the production of concavity in real basins.

Chapter 5

Multiple Grain Size Modeling Study

This chapter discusses changes in active layer texture and concavity of five simulated basins composed of heterogeneous sediment. The percentage of sand and gravel in the parent material is different in each basin, but the sand and gravel modes remain the same. Downstream fining develops in all of the basins. The equilibrium basin concavity results of the heterogeneous basins are compared with the concavity results from the homogeneous basins.

5.1 Varying Sand Content

Using equations 3.9 and 3.10 for sand and gravel transport, five basins with different parent material textures were evolved to dynamic equilibrium. The proportion of sand and gravel in the parent material differed between each run. The sand and gravel modes in every basin were 0.0005m and 0.016m, respectively. The parent material textures of the five different basins were 10%, 35%, 50%, 65% and 90% sand.

Each run began with the same flat surface with the same small amount of roughness that was used for the homogeneous experiments. Uplift across the entire basin was constant. The outlet was the only location in which water and sediment could leave the system. This outlet drained to a cell with constant elevation. The parame-

ters and domain information in Table 4.1 were also used in these basins and remained constant throughout the entire model run. All of the basins had a 3.0 meter active layer depth.

5.1.1 Downstream Fining

Figure 5-1 shows the topography of the five basins in dynamic equilibrium, shaded according to the active layer texture. The dark hillslopes have a smaller percentage of sand in the active layer than the light valleys. Although the range in proportion of sand and the exact pattern of fining in the active layer is not the same in all of the basins, the proportion of sand in the active layer always increases downstream. This can been shown graphically in plots of proportion of sand in the active layer versus contributing area (Figure 5-2, sand-area plots). The well-defined patterns of fining suggest that an analytical solution for the proportion of sand in the active layer as a function of drainage area might exist. An analytical solution has not been found, but a graphical solution will be discussed later.

In the basins with 10%, 35% and 50% sand in the parent material, there is a continuous gradual trend in fining, in contrast to the basins with 65% and 90% sand in the parent material, which have two fining trends. The change in fining trend occurs when the active layer is composed of 40% sand, marking the transition from a gravel- to sand-bed stream. For the most part, the composition of the active layer in the three coarsest basins remains between 10% and 40% sand. Even the basin with 65% sand in its parent material has an active layer texture that is between 10% and 40% sand in most areas. The active layer composition tends toward this range, whether the sand content in its active layer is reduced relative to the substrate, as in the basins with 35%, 50% and 65% sand in the parent material, or increased relative to the substrate, as in the basin with 10% sand in the parent material. In all of the basins, for a given drainage area, the active layer is coarser if the parent material is coarser.

Because all of the basins have reached equilibrium, the sediment transport rate at every cell must be just large enough to carry all of the material which has been

(a)

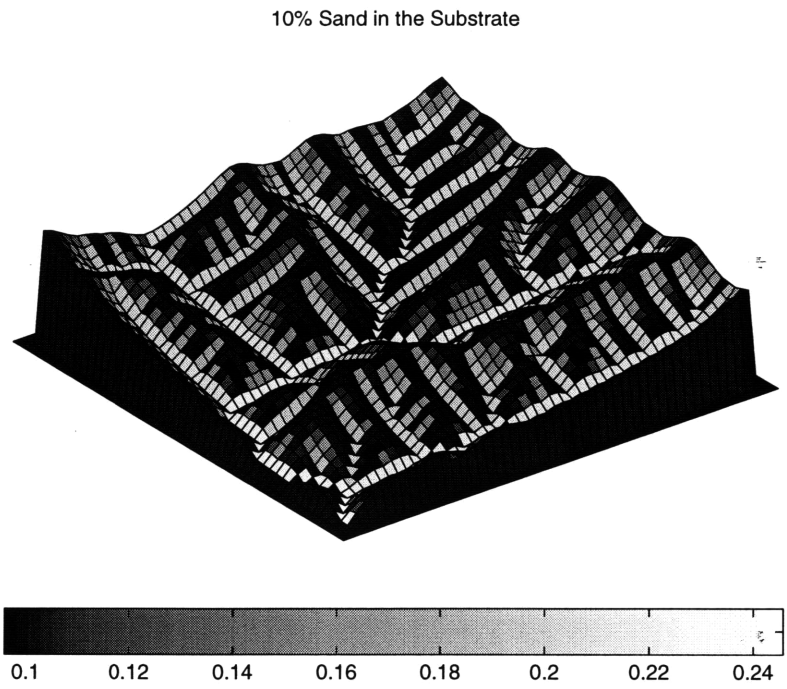
10% Sand in the Substrate
0.1
0.12
0.14
0.16
0.18
0.2
0.22
0.24

(b)

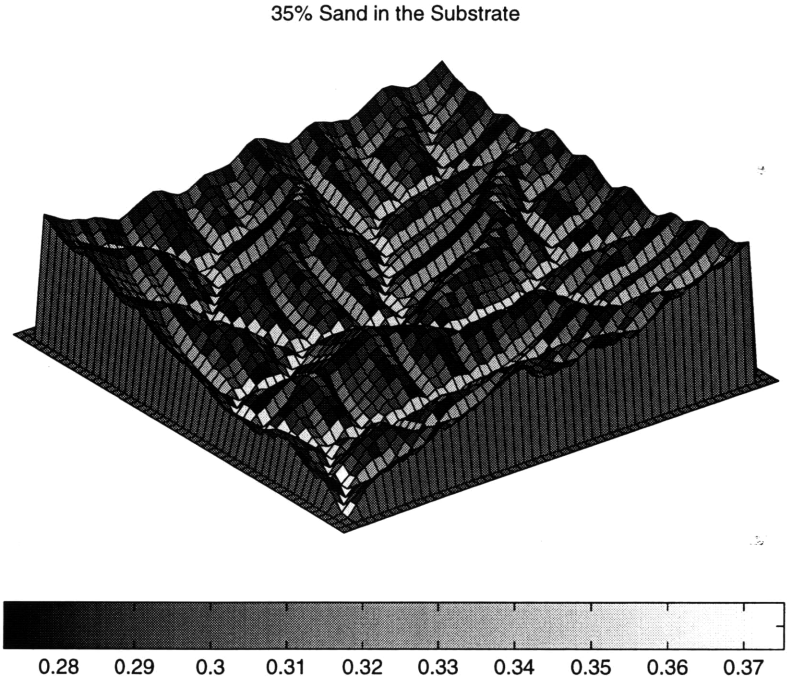
35% Sand in the Substrate
0.28
0.29
0.3
0.31
0.32
0.33
0.34
0.35
0.36
0.37

(c)

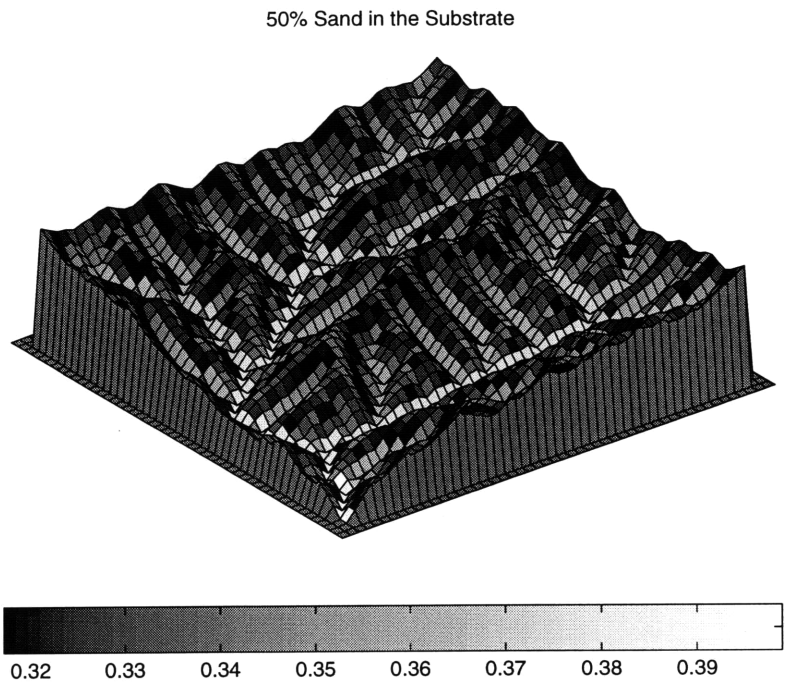
50% Sand in the Substrate
0.32
0.33
0.34
0.35
0.36
0.37
0.38
0.39

(d)

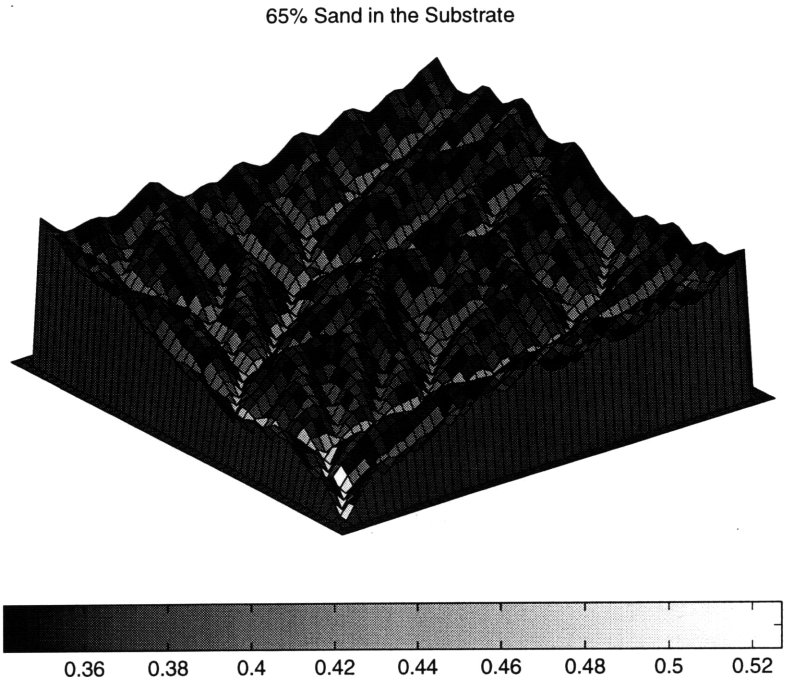
65% Sand in the Substrate
0.36
0.38
0.4
0.42
0.44
0.46
0.48
0.5
0.52

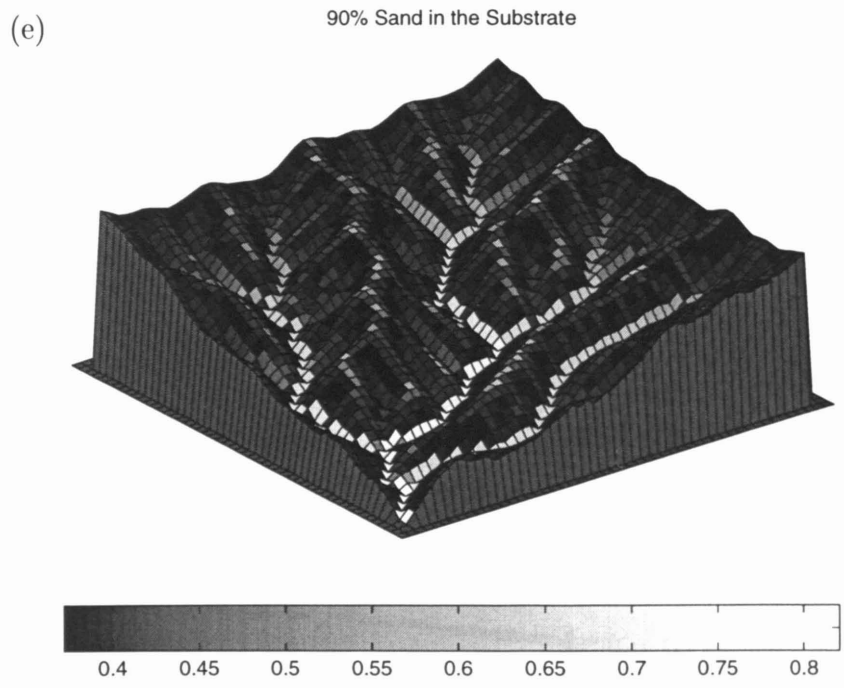

Figure 5-1: Topography of five equilibrium basins composed of different percentages of sand in the substrate. Shading is according to the proportion of sand in the active layer. Color bars show the range in proportion of sand in the active layer for each basin. Figures (a), (b), (c), (d) and (e) are for basins with 10%, 35%, 50%, 65%, and 90% sand in the substrate, respectively.

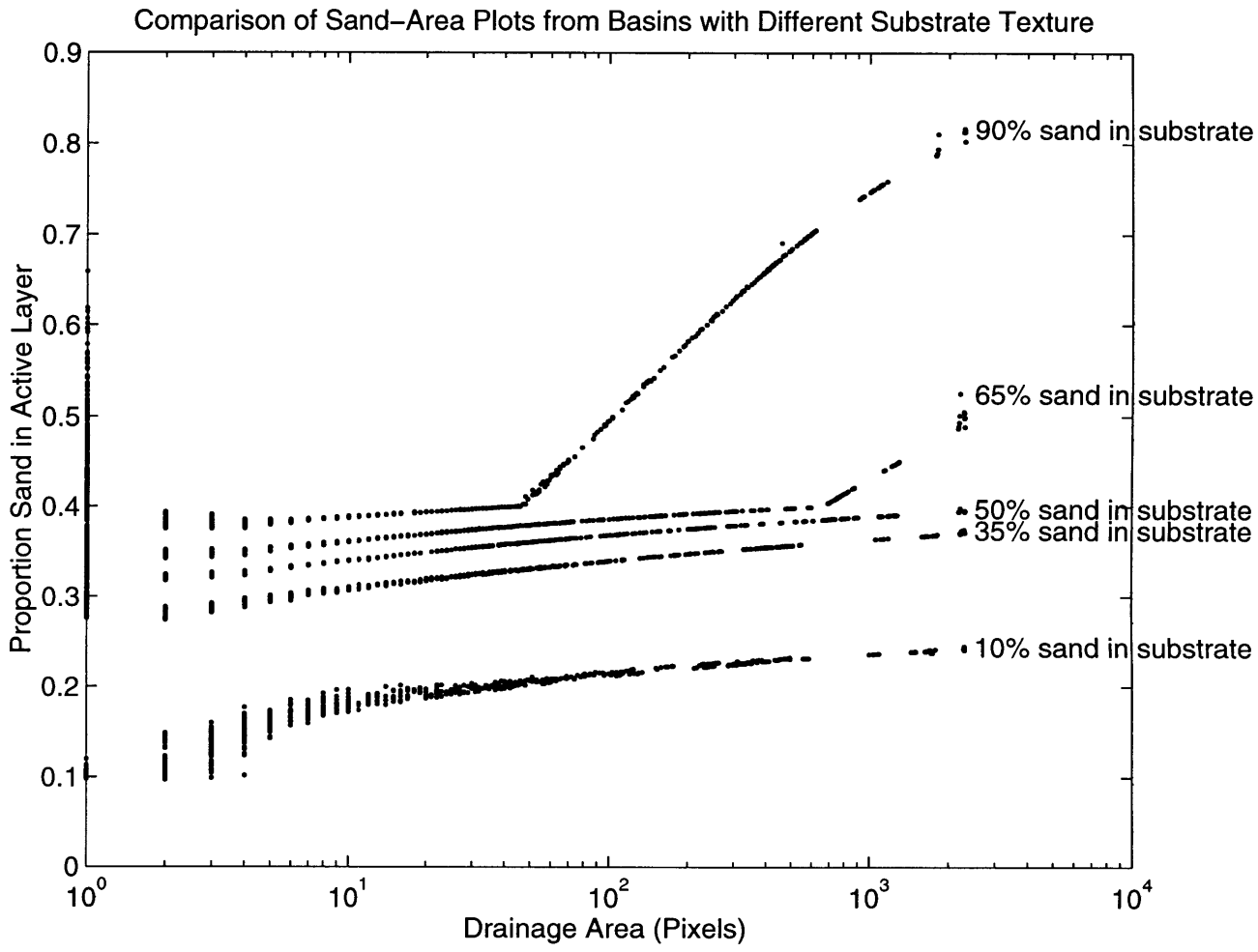

Figure 5-2: Sand-area plots for all five of the basins with different parent material textures.

"uplifted" into the basin upstream of it. The composition of the material added to the basin is that of the substrate. The equilibrium sediment transport rates for gravel and sand are therefore given by

$$Q_s^g = (1 - f_s^{sub})UA \quad \text{and} \tag{5.1}$$

$$Q_s^s = f_s^{sub}UA, \tag{5.2}$$

where f_s^{sub} is the proportion of sand in the substrate. For the simplest case where $f_s^{sub} = 0.5$, the appropriate values of f_s and S for a given drainage area are those unique values which satisfy

$$Q_s^g = Q_s^s = 0.5UA. \tag{5.3}$$

A graphical solution to equation 5.3 is used to understand the fining trend in the basin with 50% sand in its substrate. Equations 3.9 and 3.10 state that

$$Q_s^g \propto (1 - f_s)\left(\frac{\tau}{\rho}\right)^{1.5}\left[1 - \frac{\tau_{cg}}{\tau}\right]^{4.5} \quad \text{and} \tag{5.4}$$

$$Q_s^s \propto f_s\left(\frac{\tau}{\rho}\right)^{1.5}\left[1 - \sqrt{\frac{\tau_{cs}}{\tau}}\right]^{4.5}, \tag{5.5}$$

where the constant of proportionality is the same for relations 5.4 and 5.5. Figure 5-3 uses relations 5.4 and 5.5 to construct plots of Q_s^g and Q_s^s as a function of f_s for various values of τ. Since Q_s^g and Q_s^s increase systematically with drainage area, the y-axis in Figure 5-3 also represents drainage area (increasing upward). The intersection between each Q_s^g and Q_s^s for a single value of τ is highlighted, illustrating the value of f_s which satisfies equation 5.3 at a particular location in the drainage basin. The locus of the intersections of Q_s^g and Q_s^s illustrates the relation between the proportion of sand in the active layer and the sediment transport rate or, equivalently, the drainage area. For the range of τ values shown, there is a fairly constant increase in transport rate with f_s. The largest value of τ used in Figure 5-3 is also the largest shear stress value produced by the model in the basin; both the numerical and graphical model predict that the maximum value of f_s is less than 0.4. There is less of a range in the

proportion of sand in the active layer in the graphical solution than in the simulated basin because the entire range of shear stress values is not shown.

The graphical solution indicates that for a basin with $f_s^{sub} = 50\%$, given the range of shear stress values in the basin, a monotonic fining pattern develops. A similar analysis for the basins with 10% and 35% sand in the substrate also predicts a single fining trend with the appropriate range of τ values.

In the two finer basins, when the active layer texture surpasses 40% sand, the fining pattern changes, becoming much stronger. Again, this can be explained graphically. For the basin with 90% sand in its substrate, at equilibrium, $Q_s^s = 9Q_s^g$. Figure 5-4 shows plots of $9Q_s^g$ and Q_s^s for five different τ values. The locus of the intersections between $9Q_s^g$ and Q_s^s for a given τ has less of an increase with f_s than is shown in Figure 5-3. The active layer texture needs to change much more than was the case when $f_s < 0.4$ to create a small change in the transport rate, or equivalently, in the drainage area. (Figures 5-3 and 5-4 both have the same scale.) The same τ values were used in both Figures 5-3 and 5-4; these values were produced in both basins in higher drainage areas. The results are different because the relation between Q_s^g and Q_s^s differs.

Both fining patterns are shown on a single plot in Figure 5-5. The intersections of Q_s^g and Q_s^s for each τ value are highlighted, appropriate for a basin with 50% sand in its substrate. The figure clearly shows a more gradual increase in transport rate, or drainage area, once f_s surpasses 40%. This implies that when $f_s > 0.4$, the active layer texture has to change more rapidly with drainage area than it does when $f_s < 0.4$. The reason that both trends are not apparent in the modeled basin with 50% sand in the substrate, even though they are produced graphically, is because the shear stress values needed to sustain an active layer composition with greater than 40% sand were not produced in the modeled basin. The graphical results suggest that a larger basin with 50% sand in its substrate would have both fining trends (assuming the same parameters).

The origin of the break in behavior of the fining trend at $f_s = 0.4$ lies in the relationship between τ_c and f_s. The critical shear stress for both sand and gravel

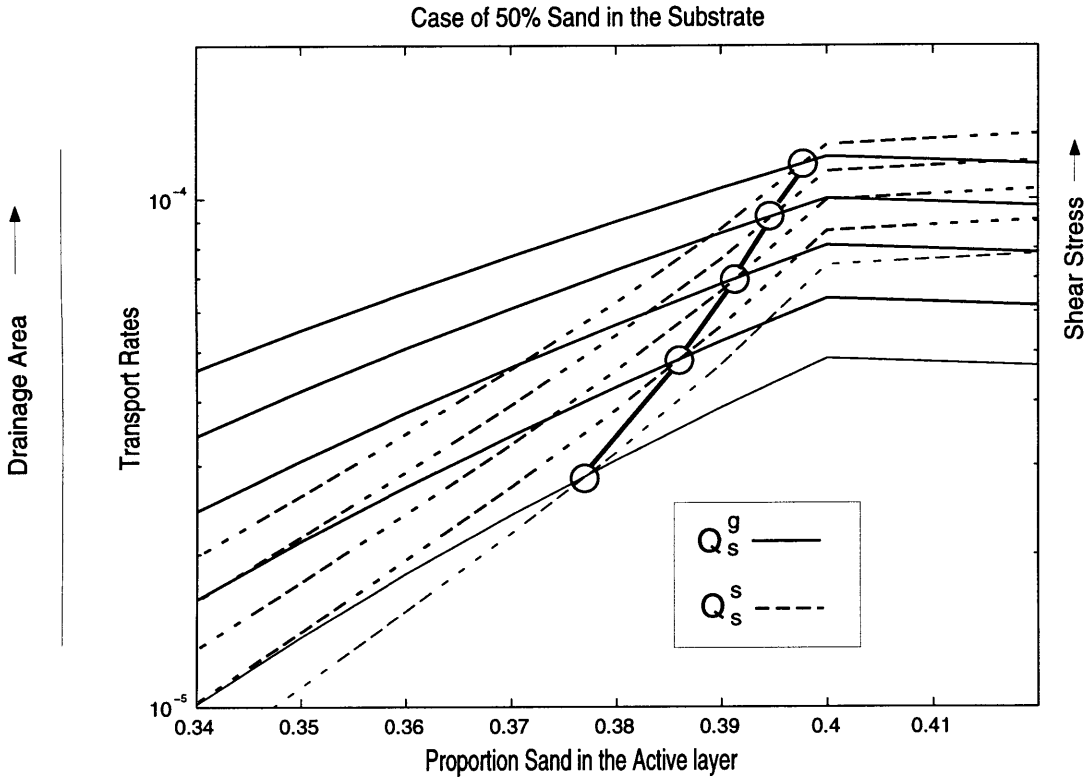

Figure 5-3: Plot of gravel (solid thin lines, labeled Q_s^g) and sand (dashed lines, labeled Q_s^s) transport rates as a function of proportion sand in the active layer. Both the gravel and sand sediment transport curves are shown for shear stress values of 6.5, 7, 7.5, 8, and $8.5\frac{\text{kg}}{\text{ms}^2}$. As shear stress increases, so does the transport rate of both gravel and sand. The circles highlight the intersection between Q_s^g and Q_s^s for a single shear stress value. The thick line between the circles illustrates a hand-drawn connection between each intersection. Because the intersection of Q_s^g and Q_s^s is shown, the thick line shows how the proportion of sand would vary as a function of drainage area in an equilibrium basin with 50% sand in the substrate.

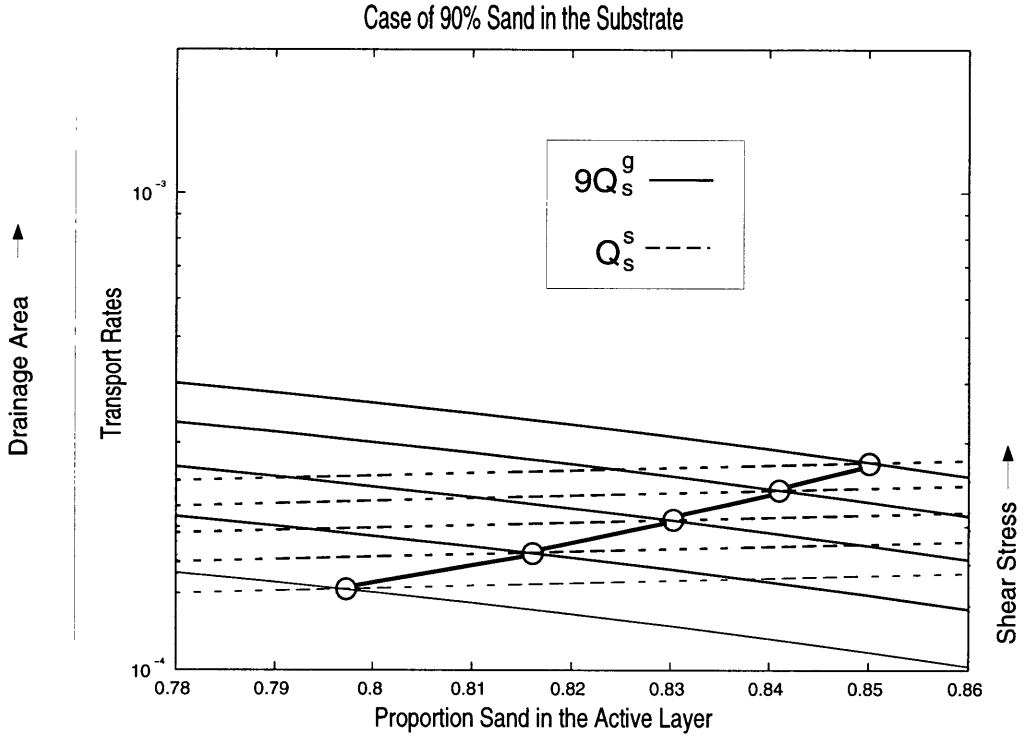

Figure 5-4: Plot of sand transport rate (dashed lines, labeled Q_s^s) and nine times the gravel transport rate (solid thin lines, labeled Q_s^g) as a function of proportion sand in the active layer. Both the gravel and sand sediment transport curves are shown for shear stress values of 6.5, 7, 7.5, 8, and $8.5\frac{\text{kg}}{\text{ms}^2}$. As shear stress increases, so does the transport rate of both gravel and sand. The circles highlight the intersection between Q_s^s and $9 * Q_s^g$ for a single shear stress value. The thick line between the circles illustrates a hand drawn connection between each intersection. Because the intersection of $9 * Q_s^g$ and Q_s^s is shown, the thick line shows the solution for changes in proportion sand in the active layer as contributing area increases in an equilibrium basin with 90% sand in the substrate.

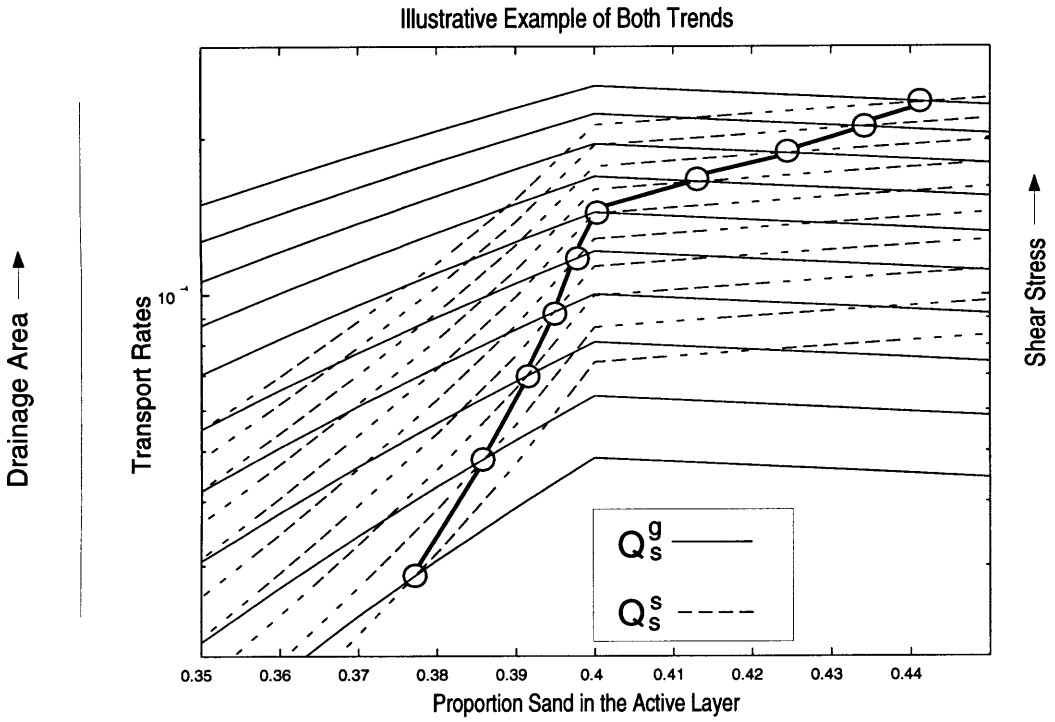

Figure 5-5: Plot of gravel (solid thin lines, labeled Q_s^g) and sand (dashed lines, labeled Q_s^s) transport rates as a function of proportion sand in the active layer. Both the gravel and sand sediment transport curves are shown for shear stress values of 6.5, 7, 7.5, 8, 8.5, 9, 9.5, 10, 10.5 and $11 \frac{\text{kg}}{\text{ms}^2}$. As shear stress increases, so does the transport rate of both gravel and sand. The circles highlight the intersection between Q_s^g and Q_s^s for a single shear stress value. The thick line between the circles illustrates a hand-drawn connection between each intersection. Because the intersection of Q_s^g and Q_s^s is shown, the thick line shows the solution for changes in proportion sand in the active layer as contributing area increases in an equilibrium basin with 50% sand in the substrate.

changes from a decreasing function of the proportion of sand in the active layer to a constant value when $f_s = 0.4$ (see Figure 2-4). Due to the nonlinear dependence of the sediment transport rate on critical shear stress, when critical shear stress is a decreasing function of f_s, small increases in f_s bring about relatively large changes in both the gravel and sand sediment transport rates. Once the critical shear stress becomes constant, larger changes in f_s are required to change the sand sediment transport rate, because Q_s^s is now only increasing linearly with f_s. However, the gravel sediment transport rate begins to decrease with f_s, once f_s increases past 0.40 and τ_{cg} becomes constant. The active layer sand content can increase past a value of 0.4 because τ increases downstream. Q_s^g is a stronger function of τ than Q_s^s (see equations 5.4 and 5.5); as f_s increases downstream causing a decrease in Q_s^g and an increase in Q_s^s, τ also increases, which has a greater impact on Q_s^g than on Q_s^s. This description of the equations does not explain the exact shape of the fining pattern, but it gives some insight into the complexity of the changes downstream.

5.1.2 Basin Concavity

Figure 5-6 shows the slope-area plots for the five heterogeneous basins. Table 5.1 shows the slope of the slope-area plot for the five basins. The slope of the least-squares best fit is calculated between drainage areas of 10 and 1000 cells. There is no trend in basin concavity with parent material texture, unlike the results from the homogeneous basins (see Table 4.2).

The basin with 90% sand in its substrate is less concave than the other basins, but it still has a reasonable morphology. Concavity in this basin changes when the drainage area is around 50 cells. The slope of the slope-area plot, if measured between drainage areas of 10 and 50 cells, is -0.44, and if measured between drainage areas of 50 and 1000 cells, is -0.24. The change in concavity occurs where the fining pattern changes (see Figure 5-2). This follows the behavior of natural systems in which the transition from gravel-bed to sand-bed stream is often marked by a discontinuity in bed slope (e.g. Ichim and Radoane (1990), Parker (1991a), and Ferguson et al. (1996)). The transition in bed-slope in the basin with 65% sand in the substrate can

Percent Sand in Substrate	10%	35%	50%	65%	90%
Slope of Slope-Area Plot	-0.37	-0.38	-0.38	-0.38	-0.31

Table 5.1: Table of concavity results for basins with two grain sizes.

not be detected even though there is a transition from coarse-bed to fine-bed stream. There are not enough cells with sand beds to detect the bed-slope transition.

The four basins with almost identical concavities have different substrate textures, but, for the most part, they all have active layer textures between 10% and 40% sand. The surface texture, not the substrate texture, governs sediment transport. The adjustment of the active layer texture allows for reasonable concavity results, regardless of the substrate texture. Without the adjustment of the active layer texture, the sand-sized homogeneous basins failed to produce reasonable morphologies.

5.1.3 Sensitivity of the Active Layer Depth

The concavity results depend on the texture of the active layer. It is important that the active layer texture doesn't dependent on the depth of the active layer, which was imposed as an independent parameter. If the active layer texture were to vary with active layer depth, the results of the model would be less generalizable.

Sensitivity tests show that the depth of the active layer does not greatly affect the results, unless the active layer depth is made very small. The drainage networks, slope-area plots, and sand-area plots of two basins with different active layer depths (1.0m and 0.5m) are shown in Figures 5-7, 5-8, and 5-9, respectively. The substrate of both basins contains 65% sand. These basins were evolved using the same parameters as in Table 4.1 and the same initial surface which was used for all of the previous runs. The results of these two runs can also be compared with the basin with 65% sand in its substrate and a 3.0 meter active layer that was discussed earlier in this chapter. Downstream changes in grain size and basin concavity were not affected significantly by the change in active layer depth. In fact the concavity (when measured between 10 and 1000 cells) of all of the basins is the same. The shape of the network varies

(a)

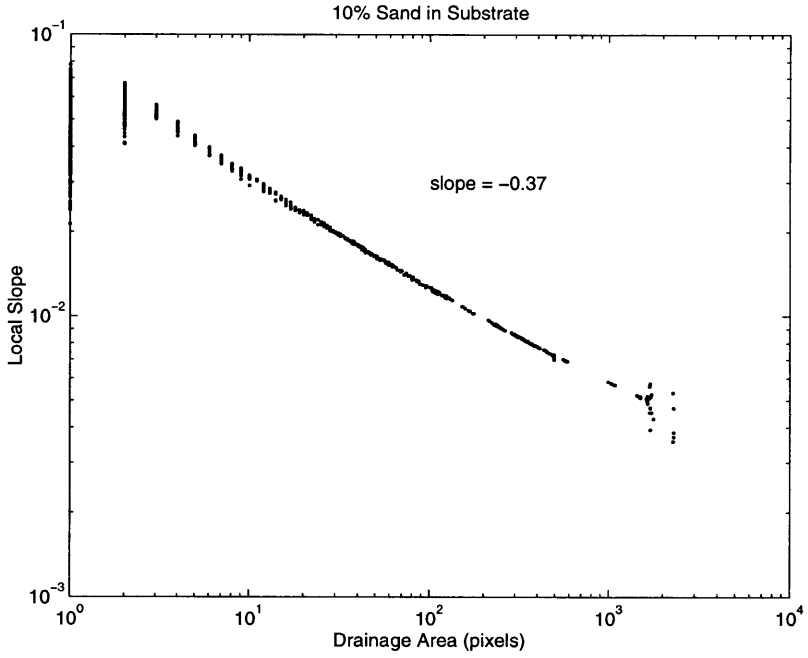
10% Sand in Substrate
slope = −0.37
Local Slope
Drainage Area (pixels)

(b)

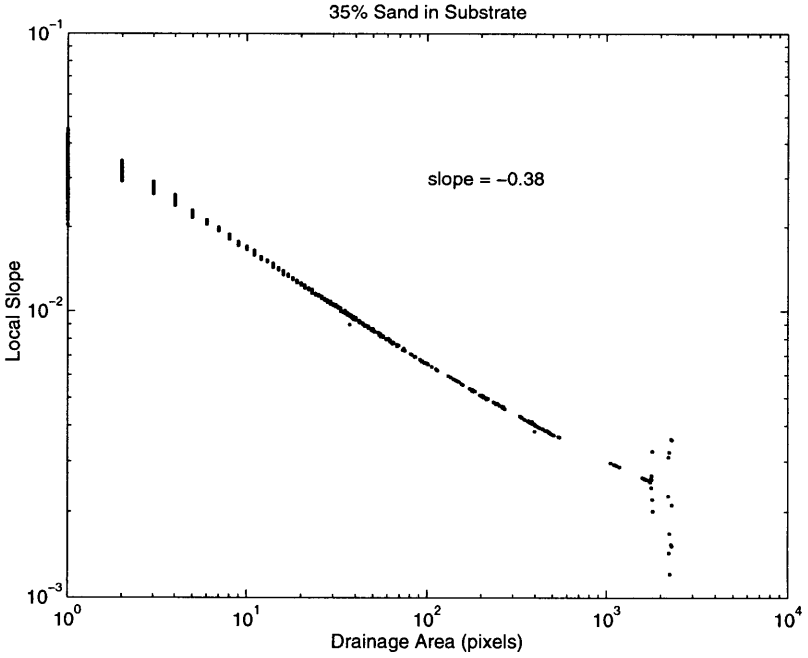
35% Sand in Substrate
slope = −0.38
Local Slope
Drainage Area (pixels)

(c)

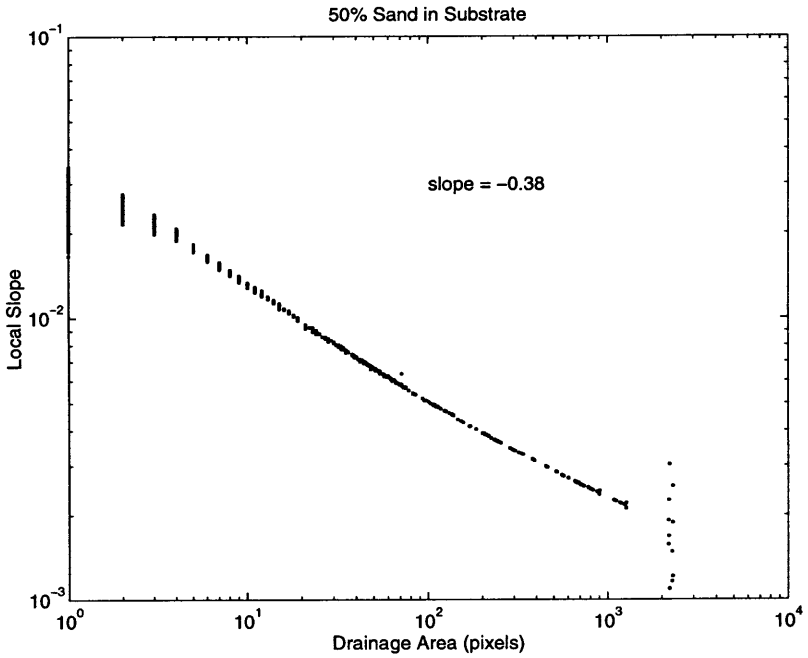
50% Sand in Substrate
slope = −0.38
Local Slope
Drainage Area (pixels)
10^{-1}
10^{-2}
10^{-3}
10^{0}
10^{1}
10^{2}
10^{3}
10^{4}

(d)

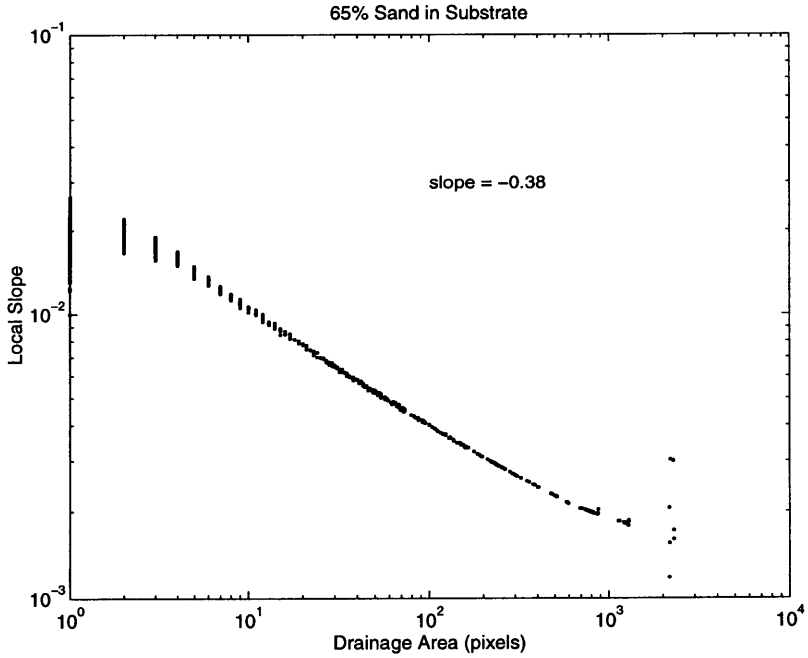
65% Sand in Substrate
slope = −0.38
Local Slope
Drainage Area (pixels)
10^{-1}
10^{-2}
10^{-3}
10^{0}
10^{1}
10^{2}
10^{3}
10^{4}

(e)

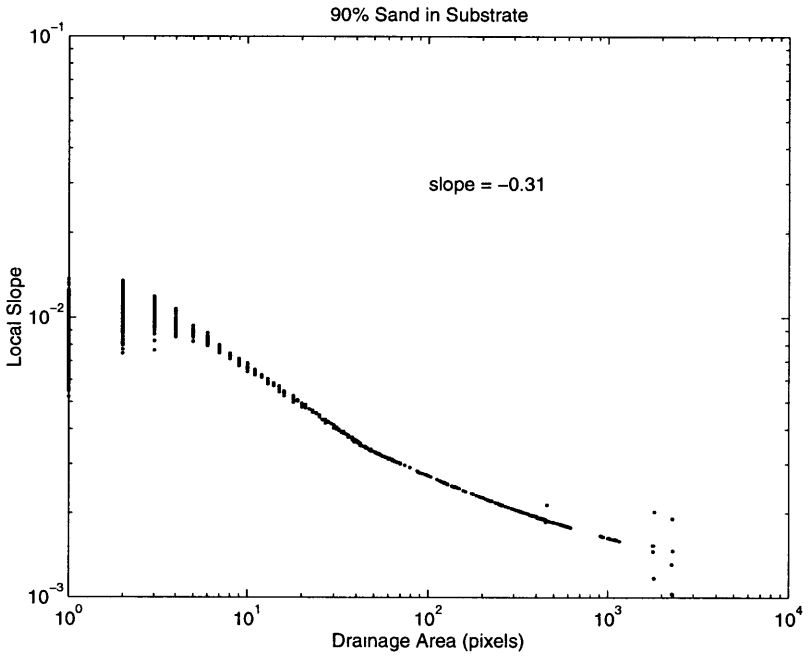

Figure 5-6: Slope-area relationships of basins composed of different material in the substrate. The value of slope given is from a linear fit to the data for drainage area between 10 and 1000 cells. Figure (a), (b), (c), (d) and (e) are for basins with 10%, 35%, 50%, 65%, and 90% sand in the substrate, respectively.

slightly, which is expected since the channel network has been shown to be very sensitive to small changes in the boundary conditions (Ijjasz-Vasquez et al. 1992).

5.2 Discussion

Because the basins are in dynamic equilibrium, there are no changes in either active layer texture or elevation in time. The uplift rate and the substrate texture are constant throughout, implying that the rate of erosion of each grain size is constant as well. Even though the texture of the active layer varies across the basin, the rate of erosion does not. Although it may be counter intuitive, the variation in surface texture downstream is a necessary adjustment for the basin to reach equilibrium. In the heterogeneous basins, both the local slope and the surface texture adjust at every cell, allowing for an extra degree of freedom relative to the homogeneous basins. The adjustment of active layer texture is what allows for reasonable concavities.

Downstream fining has been observed in the field, in flume studies, and in modeling experiments of both gravel- and sand-bed streams. The Allt Dubhaig, Scotland, is one example in which downstream fining of river gravel has been observed and successfully modeled (Hoey and Ferguson (1994), Ferguson et al. (1996), and Hoey and Ferguson (1997)). Pebble counts and bulk samples showed that median grain size decreased by approximately 80% along the 2.5km reach. Laboratory abrasion tests of the same sediment show only a 0.1% reduction in median grain size over the equivalent length of reach. This implies that in the Allt Dubhaig, sorting during bedload transport and deposition is the predominant cause of fining. Use of a one-dimensional model supports their observations. The model shows that fining develops quickly over an initially uniform bed as a wave of bedload finer than the bed moves downstream along a concave profile. Once the stream reaches equilibrium the pattern of fining will disappear because fluvial discharge does not vary downstream.

Fining rates comparable to those observed in natural gravel rivers have been produced in flume studies (Paola et al. (1992) and Seal et al. (1997)). Downstream fining was found to require only the transport and deposition of a sufficiently poorly sorted

(a)

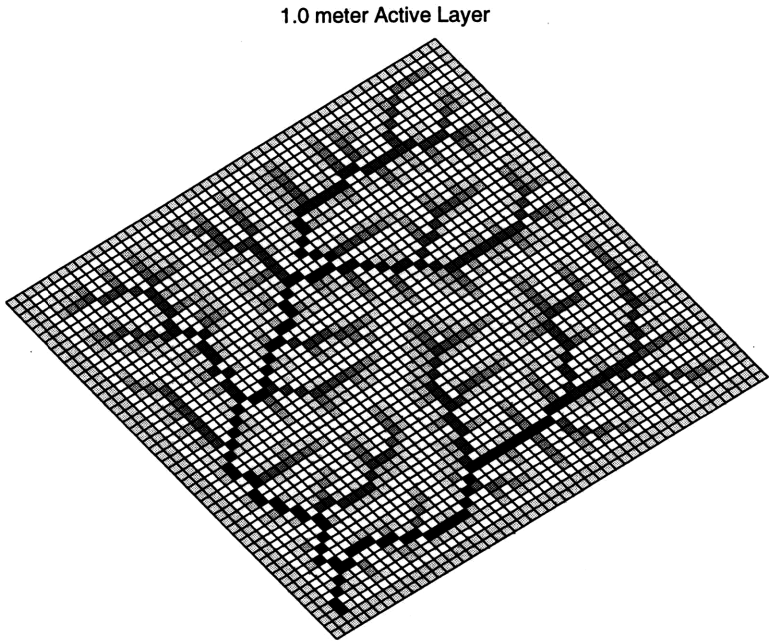

(b)

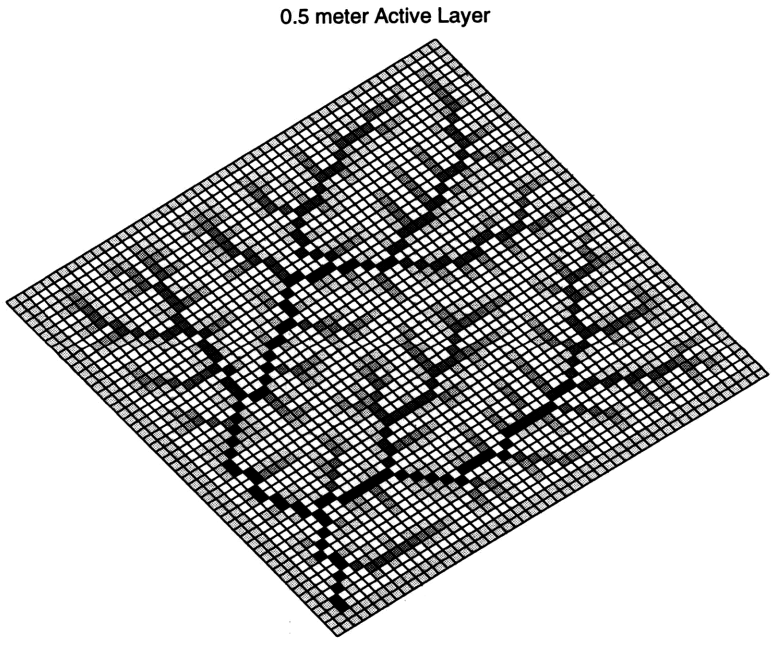

Figure 5-7: The drainage networks produced using a 1.0m active layer depth (a) and a 0.5m active layer depth (b).

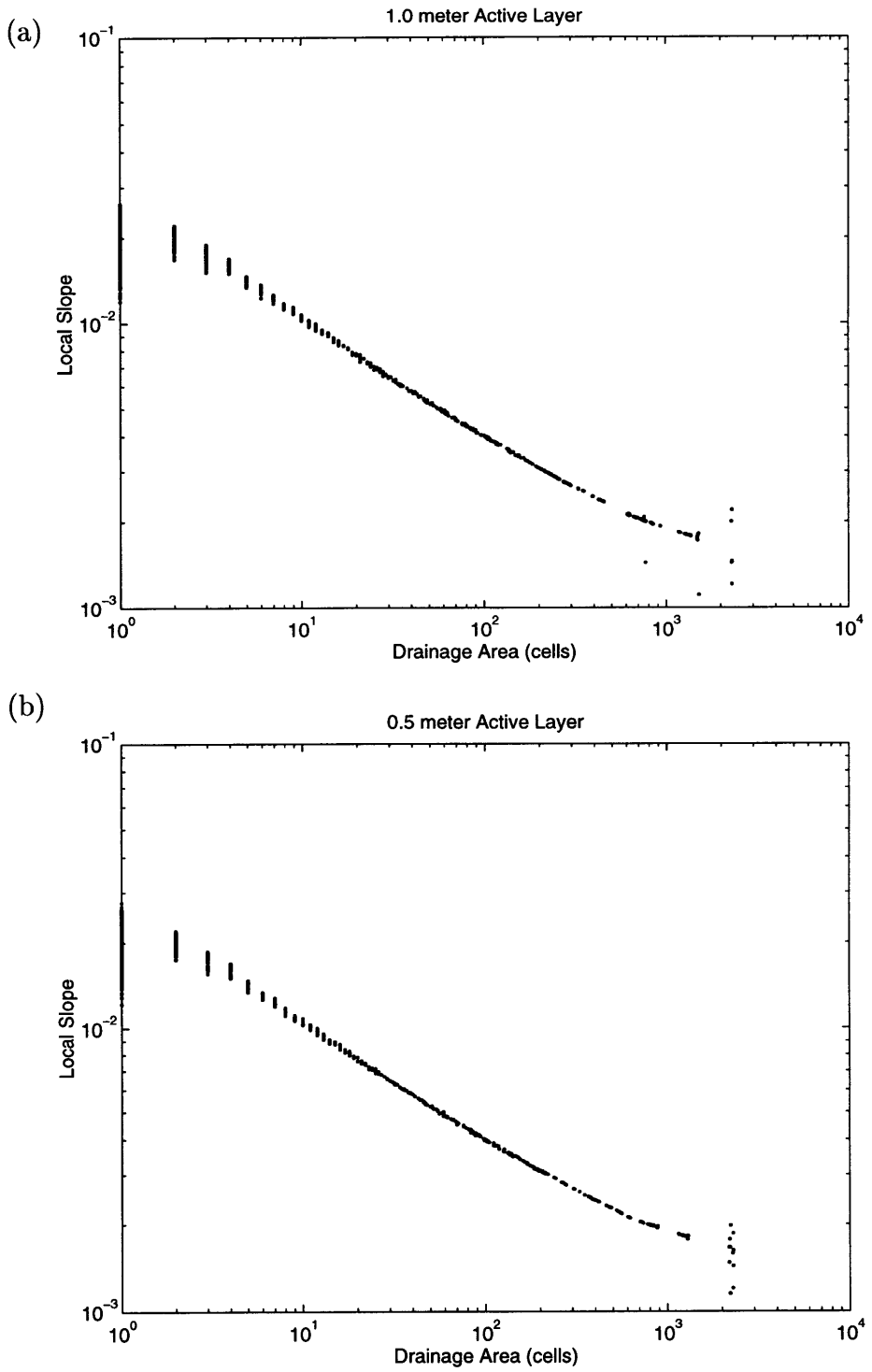

Figure 5-8: The slope-area relationships produced using a 1.0m active layer depth (a) and a 0.5m active layer depth (b).

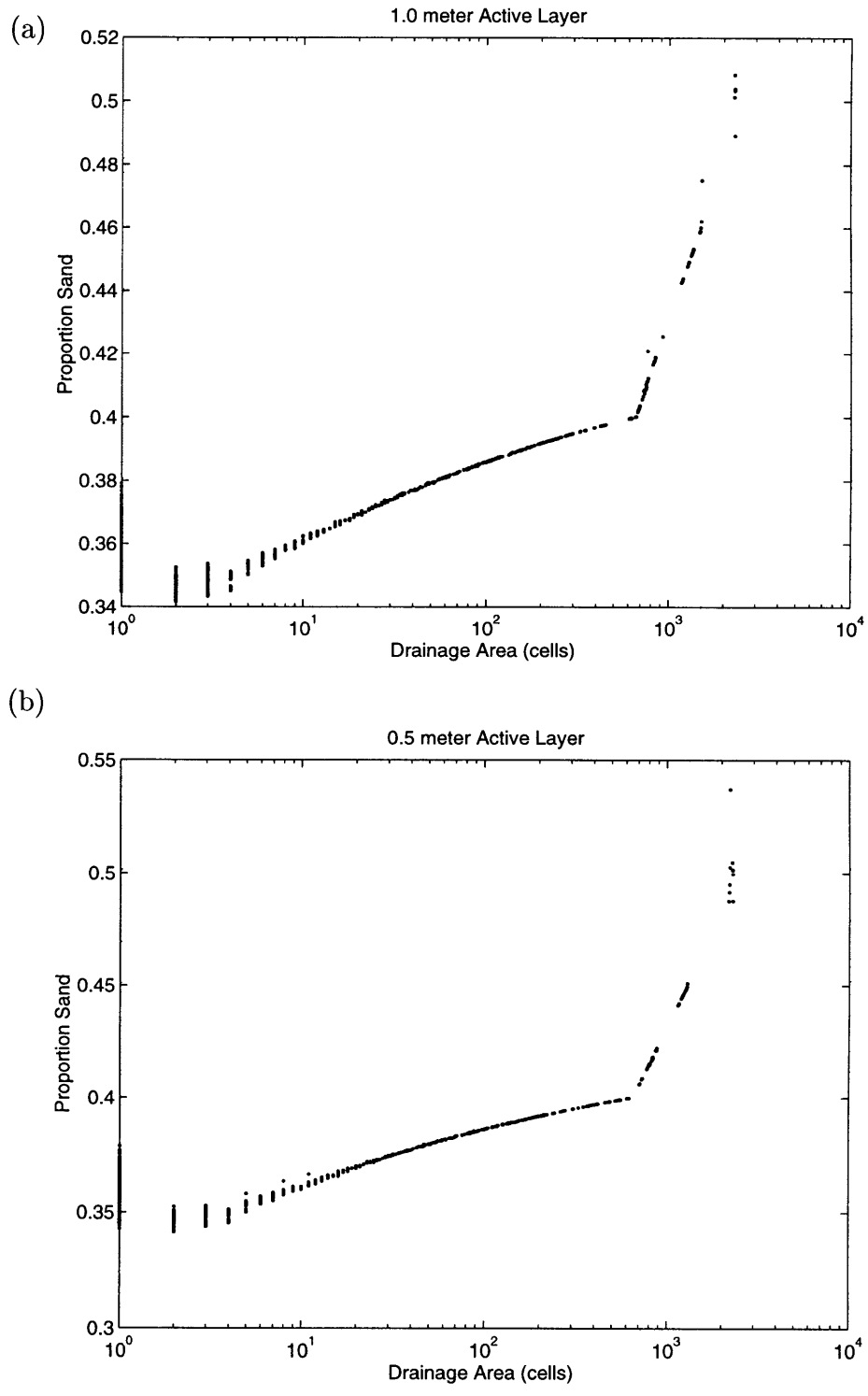

Figure 5-9: This figure shows the sand-area plots produced using a 1.0m active layer depth (a) and a 0.5m active layer depth (b).

or bimodal gravel. The length of the flume was small enough to rule out abrasion. Pre-existing slope variations and variations in discharge were not necessary to produce fining. Slope variations were observed to occur at the transition from gravel- to sand-bed reaches. Decreasing slope downstream resulted from a decrease in both total load (from deposition) and grain size (from selective deposition).

A discontinuity in longitudinal profile at the transition from gravel- to sand-bed has been observed in natural rivers. In his study of river profiles and grain-size changes, Yatsu (1955) describes seven rivers in Japan which changed from a coarse-grained to a fine-grained bed at the point where river concavity changed. The change from gravel- to sand-bed was abrupt in all seven of the rivers. River morphology has been observed to vary with median grain size on a number of other rivers including the Allt Dubhaig, Scotland (Ferguson et al. 1996), the Ok Tedi, Papua New Guinea (*Sediment transport geochemestry* 1989), and the Siret, Romania (Ichim and Radoane 1990)) and in flume studies (Paola et al. (1992) and Seal et al. (1997)). Two of the simulations presented in this chapter exhibited an abrupt transition from coarse to fine active layer. In one of these basins, concavity changed with active layer texture. The change in concavity at the gravel-sand transition results from a fundamental change in the relationship between transport rate and bed textures, as predicted by the equations developed by Wilcock (1997). The transition in the bed from framework-supported to matrix-supported causes the change in the transport relationship.

In previous studies, downstream fining has been explained by abrasion and selective sorting (selective entrainment, transport and deposition of grain sizes) with an emphasis on deposition. This study revealed that downstream fining can occur under conditions other than selective deposition; the natural adjustment of the active layer to erosion can also cause downstream fining. This study confirms that abrasion is not necessary for downstream fining. Downstream fining persists during equilibrium conditions, contrary to previous studies which limit fining to transient conditions (e.g. Ferguson et al. (1996)).

Although numerous modeling studies examine grain size changes along a river reach (e.g. Borah et al. (1982a), Borah et al. (1982b), Armanini (1992), Hoey and

Ferguson (1994), Ferguson et al. (1996), Hoey and Ferguson (1997), Parker (1991a), Parker (1991b), van Niekerk et al. (1992), and Vogel et al. (1992)), there are few studies on grain size changes throughout an entire basin. Two-dimensional channel models can capture changes in grain size along a reach, but they have not been linked with the hillslopes that provide the channels with a sediment load and fluvial discharge. Pizzuto (1992) combined a watershed model and hydraulic geometry equations to quantify changes in a network of gravel-bed streams at equilibrium. The temporal evolution of the network was not simulated. The model assumed that all bedload was supplied from zero-order channels, and the rate of bedload fed into every reach was assumed to be the same. The watershed model determined bedload, water discharge, and a single grain size. Once fed into the network, grains in transport were reduced in size according to a power law. The model was calibrated to a site in the Valley and Ridge area of Pennsylvania. It was successful in capturing changes in the network, but the necessary equilibrium time scale was not realistic for the area. Pizzuto (1992) concluded that time-dependent models are better for representing fluvial systems.

In contrast to past work, this study uses a three-dimensional physically-based model to study the sediment distribution throughout an entire basin. Downstream fining is not imposed; the system naturally adjusts to create downstream fining. Sediment input to the channels is determined through the natural adjustment of the system. Tributaries are not imposed but form during the evolution of the basin. The natural interaction of hillslopes and channels adds an element which was missing from previous downstream fining studies.

Chapter 6

Preliminary Study of Climate Change

The texture of alluvial valley fill deposits has been used to infer climate change in many field studies. These studies draw a cause and effect relationship between climate change and valley morphology, in order to predict the changes caused by environmental perturbations such as deforestation or flooding. However, many field studies disagree on the influence of climate change on the texture of alluvial valley fills. Climate change is explored in this modeling study by increasing the effective precipitation rate in a simulated basin. Changes in the active layer texture in both the transient state and in the new equilibrium are discussed. The deposition of coarse sedimentary layers below the active layer is illustrated. Finally, changes in basin concavity are discussed.

6.1 Increasing Precipitation

Climate change was modeled by increasing the precipitation rate in a basin which had already reached dynamic equilibrium. A basin with 35% sand in its substrate was evolved with a 1.0m active layer depth; other than active layer depth, all of the parameters were the same as those used for the heterogeneous basins discussed in Chapter 5. The maximum depth for layers below the active layer was 0.5m. Once the

basin reached dynamic equilibrium, the effective precipitation rate was increased from 0.3m/yr to 1.5m/yr. The large increase was chosen so that the most extreme effects could be studied. The time step was decreased to 0.005 years to ensure numerical stability.

6.1.1 Transient Effects

The active layer texture is immediately changed by the increase in precipitation. Figure 6-1 shows the initial topography and topography at six later times shortly after the precipitation increase. The topography is shaded according to the proportion of sand in the active layer; the range in texture is the same for all of the plots. Figure 6-2 shows the sand-area plot before the precipitation increase and at six later times shortly after the precipitation increase. The initial pattern of fining quickly changes and is almost erased (compare Figures 6-1 (a) and 6-2 (a) with Figures 6-1 (b) and 6-2 (b)). Erosion in the upper reaches of the network causes the active layer to become finer while the lower reaches are filled in with the coarse material eroded from the upper reaches. More coarse material is able to be carried from the headwaters because fluvial discharge has increased causing bed shear stress to increase. In some regions erosion in the upper reaches of the network causes them to become finer than the valleys below, which are still covered with coarse material, and downstream coarsening develops (see Figures 6-1 (c) and 6-1 (d) and 6-2 (c) and 6-2 (d)). There is still a lot of scatter in the sand-area plots, especially in the headwaters. The scatter in active layer texture in low drainage areas persists while the valleys start to fine again (Figure 6-2 (f) and (g)).

Downstream fining of the active layer begins to re-establish itself in the tributaries about 150 years after the precipitation increase. The sand content of the active layer in cells with larger drainage areas increases at a greater rate than the sand content in cells with smaller drainage areas. This fining of the active layer is illustrated in Figures 6-2 (c), (d), (e), (f), and (g). For a given drainage area, the average sand content in the active layer increases in time from 100 to 300 years after the precipitation increase. Table 6.1 illustrates the change in the average active layer

	100yr	150yr	200yr	250yr	300yr
10cells	0.30	0.33	0.35	0.35	0.36
20cells	0.30	0.34	0.36	0.37	0.37
30cells	0.28	0.31	0.34	0.36	0.37

Table 6.1: Table of the average value of proportion sand in the active layer for three different drainage areas at five different times after the increase in precipitation.

texture for three different drainage areas through time. Different tributaries begin to fine at different times. Animation of the sequence shown in Figure 6-1 reveals that pulses of fine material from the tributaries move down the trunk stream and get buried again in coarse material from other areas.

The layers in a few nodes of a typical tributary are shown in Figure 6-3. The layering pattern is shown before the increase in precipitation and at seven later times. Initially there are no extra layers in the tributary because the system has evolved to an erosional steady state. The active layer in the upper part of the stream is coarse and becomes finer downstream. Forty years after the precipitation increase, a coarse layer of sediment has been deposited along the entire length of the tributary. (The layers indicate deposition has occurred.) All of the layers, including the active layer, are coarser than the parent material. One hundred years after the precipitation increase, erosion in the upper reaches has caused the active layer to become finer. The lower reaches are still aggrading, and they remain coarse. Fining of the active layer starts to move in a wave downstream 140 years after the precipitation increase. The entire stream has a fine surface layer 180 years after the precipitation increase. The surface layer is finer than at the start of the experiment. The coarse layers which were deposited at the beginning of the experiment still remain even after the active layer becomes fine again.

Simulation of a single climate change produces a series of different textural changes through time. The increase in precipitation caused a coarsening of the surface, deposition of a coarse sedimentary layer and eventually a surface texture which is finer than the initial one. The results indicate that the texture of alluvial deposits can not

(a)

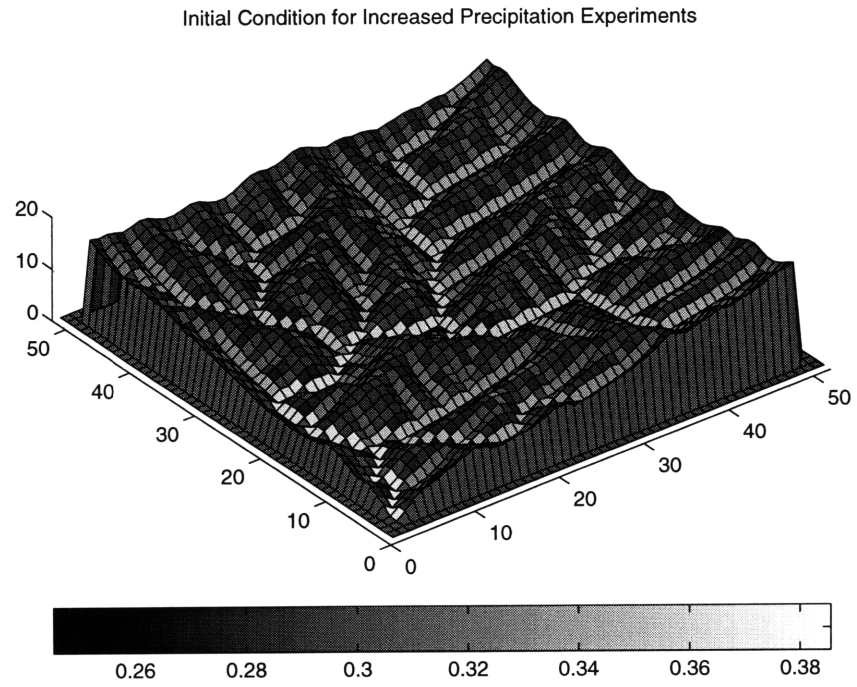
Initial Condition for Increased Precipitation Experiments
20
10
0
50
40
30
20
10
0
0
10
20
30
40
50
0.26
0.28
0.3
0.32
0.34
0.36
0.38

(b)

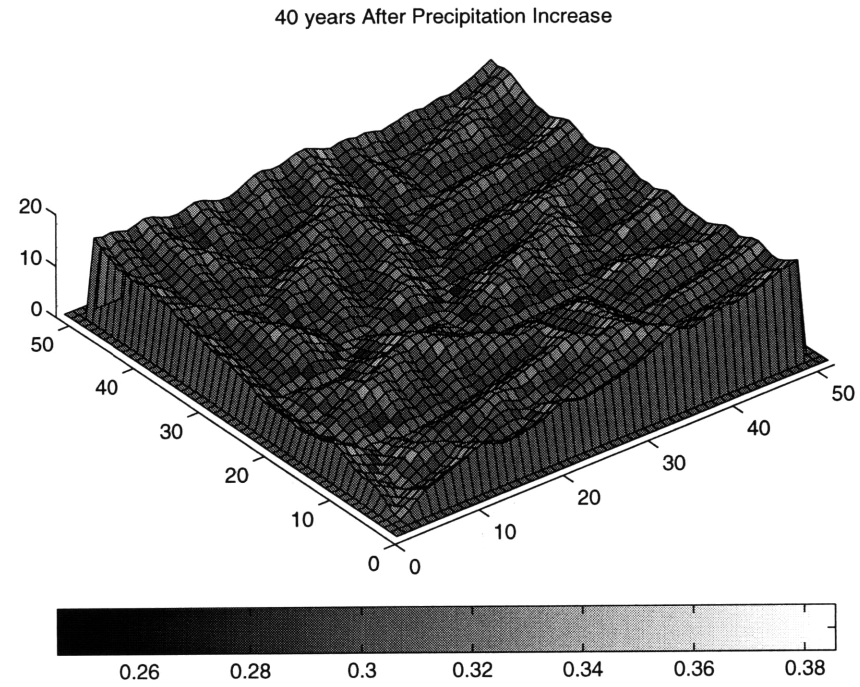
40 years After Precipitation Increase
20
10
0
50
40
30
20
10
0
0
10
20
30
40
50
0.26
0.28
0.3
0.32
0.34
0.36
0.38

(c)

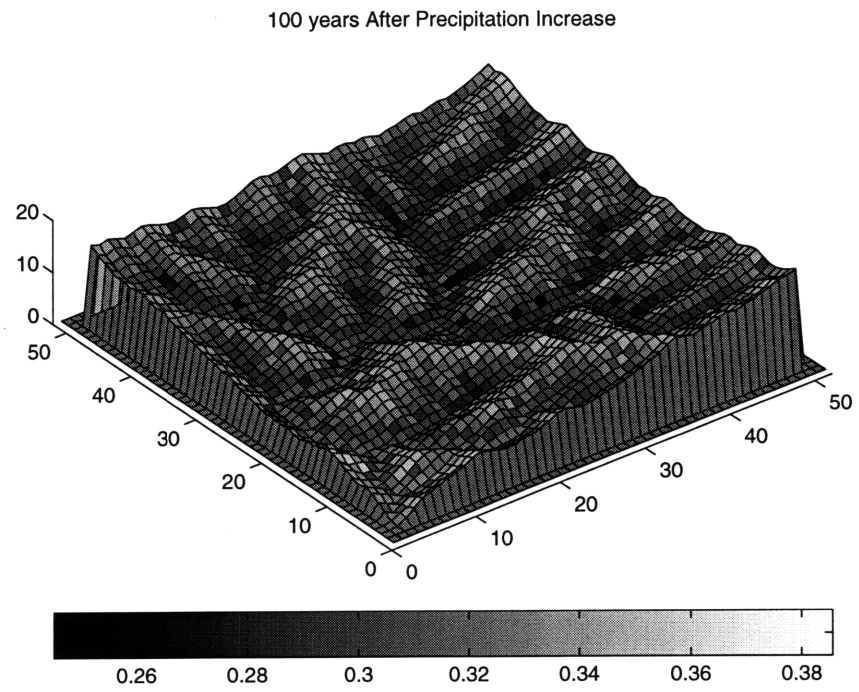
100 years After Precipitation Increase
20
10
0
50
40
30
20
10
0
0
10
20
30
40
50
0.26
0.28
0.3
0.32
0.34
0.36
0.38

(d)

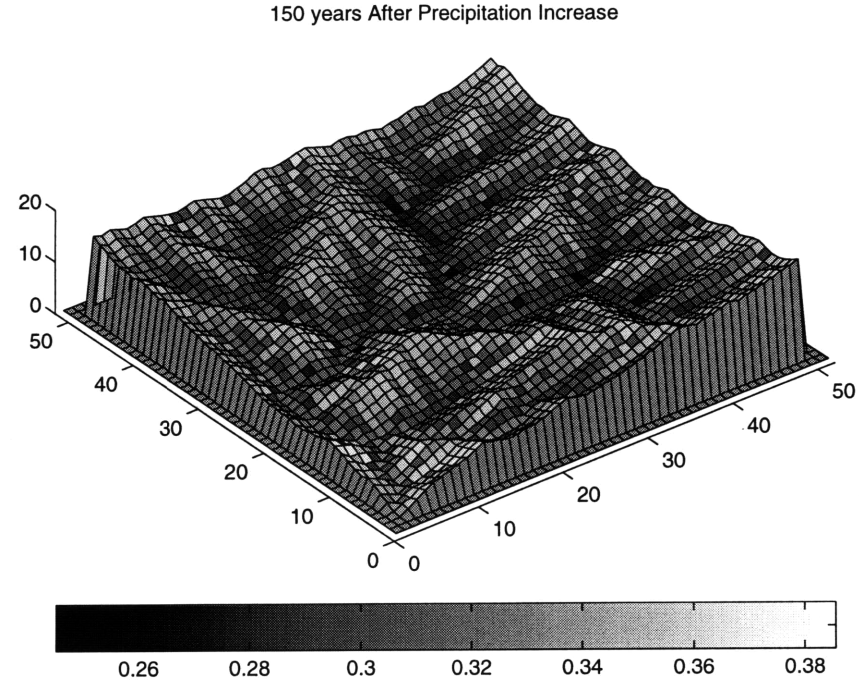
150 years After Precipitation Increase
20
10
0
50
40
30
20
10
0
0
10
20
30
40
50
0.26
0.28
0.3
0.32
0.34
0.36
0.38

(e)

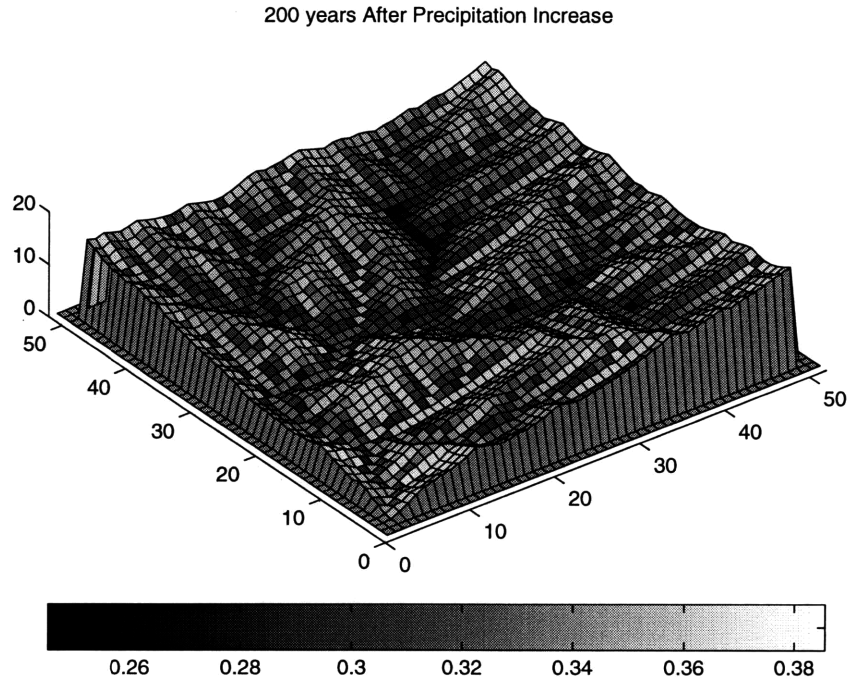
200 years After Precipitation Increase
20
10
0
50
40
30
20
10
0
0
10
20
30
40
50
0.26
0.28
0.3
0.32
0.34
0.36
0.38

(f)

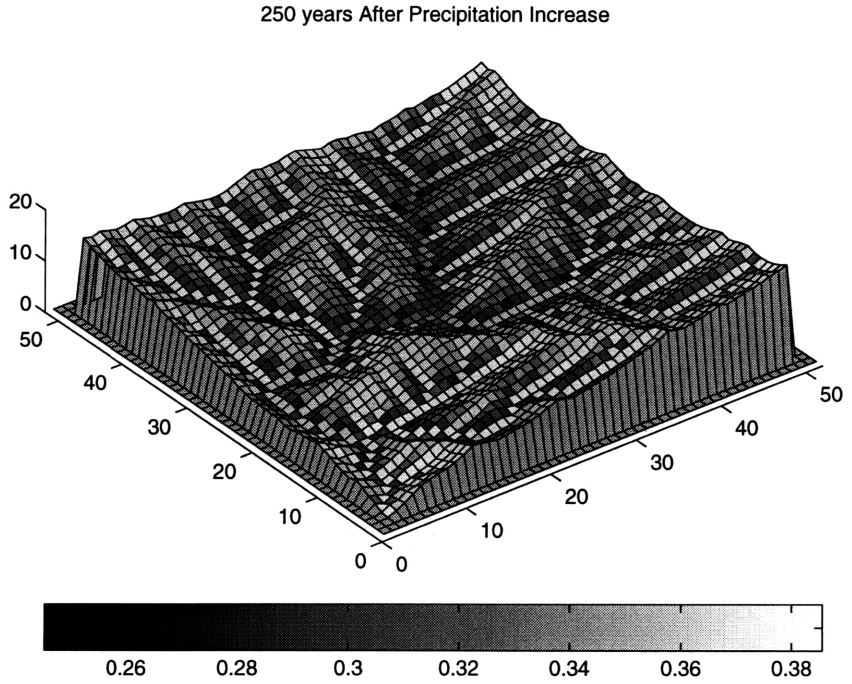
250 years After Precipitation Increase
20
10
0
50
40
30
20
10
0
0
10
20
30
40
50
0.26
0.28
0.3
0.32
0.34
0.36
0.38

(g)

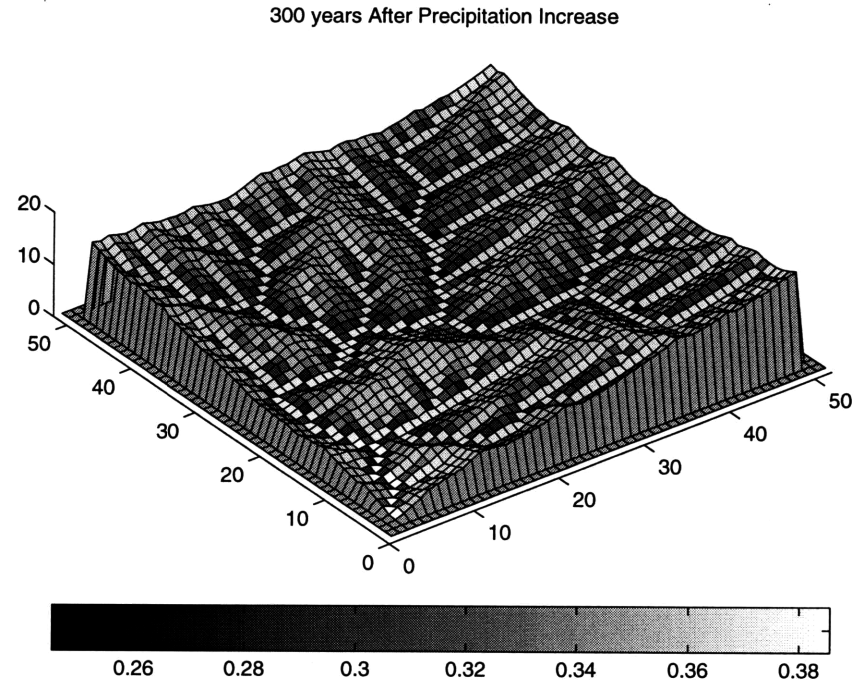

Figure 6-1: Topography of the basin at seven different times. Shading is according to the proportion of sand in the active layer. Figure (a) shows the initial condition for the run with increased precipitation. Figures (b), (c), (d), (e), (f) and (g) shows the adjustment of the basin to the increased precipitation at six different times.

(a)

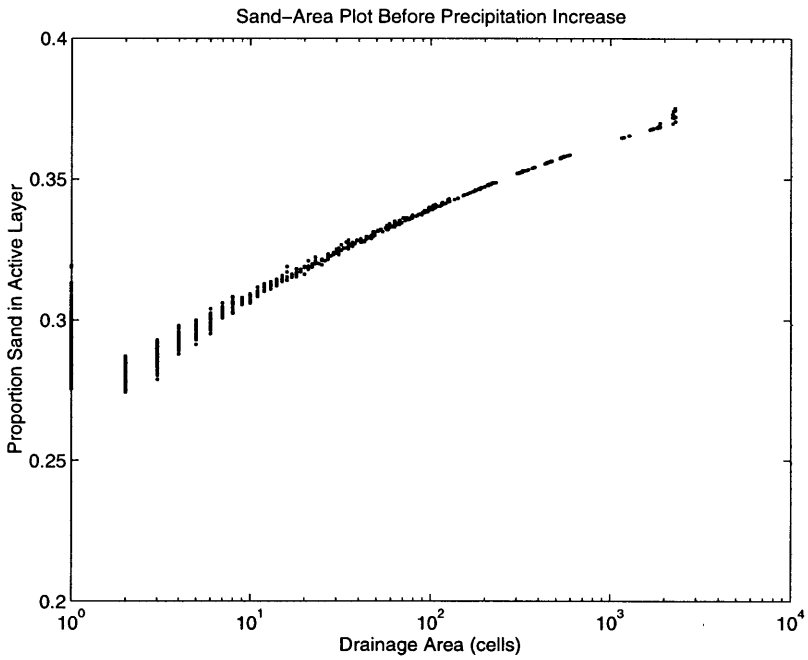
Sand–Area Plot Before Precipitation Increase
Proportion Sand in Active Layer
0.4
0.35
0.3
0.25
0.2
10^0
10^1
10^2
10^3
10^4
Drainage Area (cells)

(b)

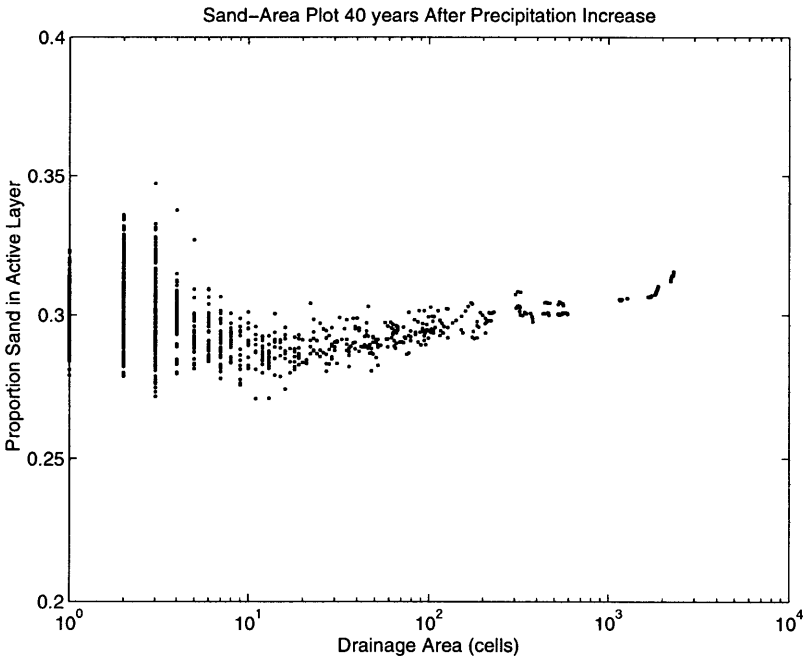
Sand–Area Plot 40 years After Precipitation Increase
Proportion Sand in Active Layer
0.4
0.35
0.3
0.25
0.2
10^0
10^1
10^2
10^3
10^4
Drainage Area (cells)

(c)

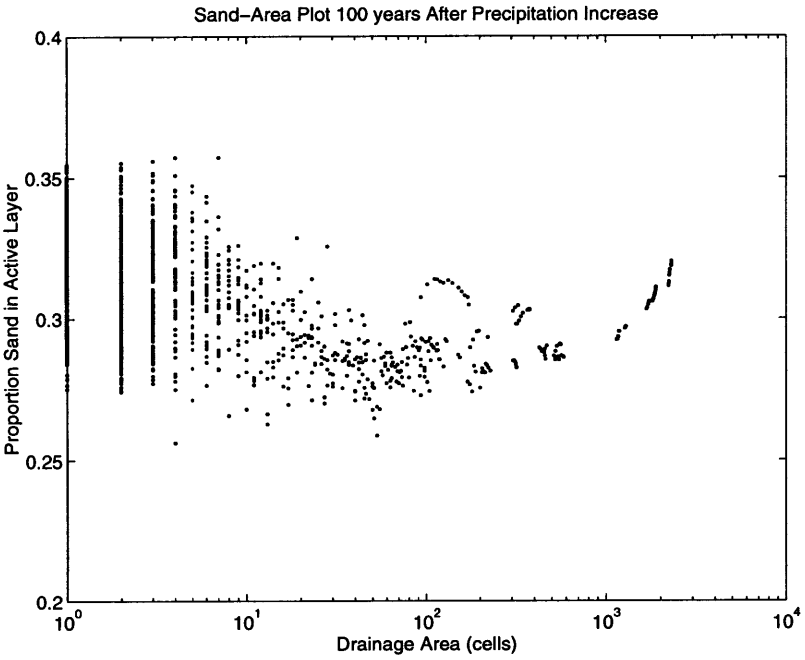
Sand–Area Plot 100 years After Precipitation Increase
Proportion Sand in Active Layer
0.4
0.35
0.3
0.25
0.2
10^0
10^1
10^2
10^3
10^4
Drainage Area (cells)

(d)

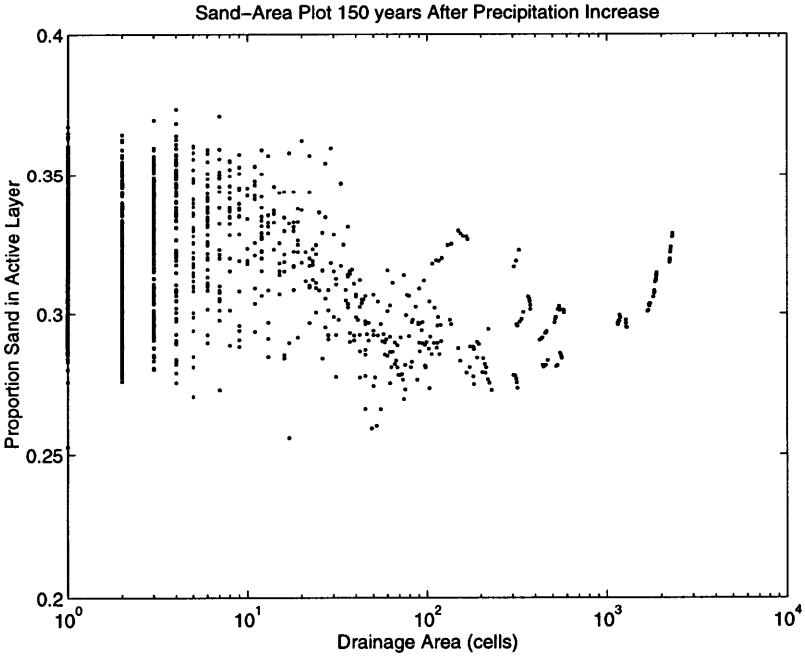
Sand–Area Plot 150 years After Precipitation Increase
Proportion Sand in Active Layer
0.4
0.35
0.3
0.25
0.2
10^0
10^1
10^2
10^3
10^4
Drainage Area (cells)

(e)

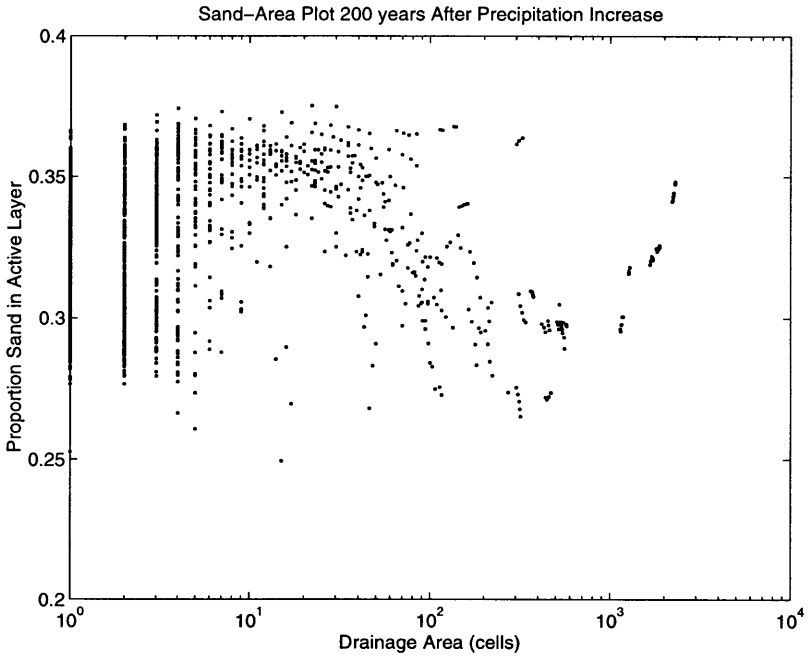
Sand–Area Plot 200 years After Precipitation Increase
Proportion Sand in Active Layer
0.4
0.35
0.3
0.25
0.2
10^0
10^1
10^2
10^3
10^4
Drainage Area (cells)

(f)

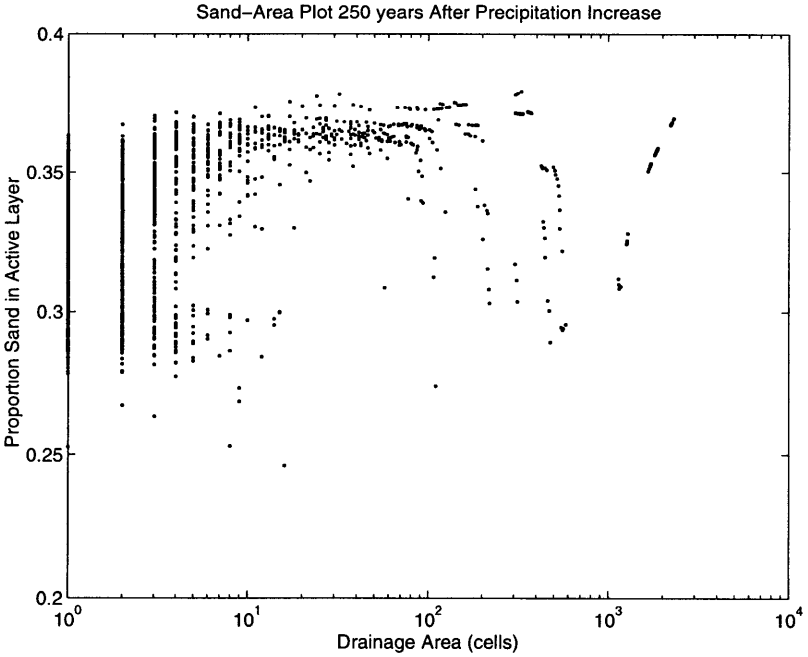
Sand–Area Plot 250 years After Precipitation Increase
Proportion Sand in Active Layer
0.4
0.35
0.3
0.25
0.2
10^0
10^1
10^2
10^3
10^4
Drainage Area (cells)

(g)

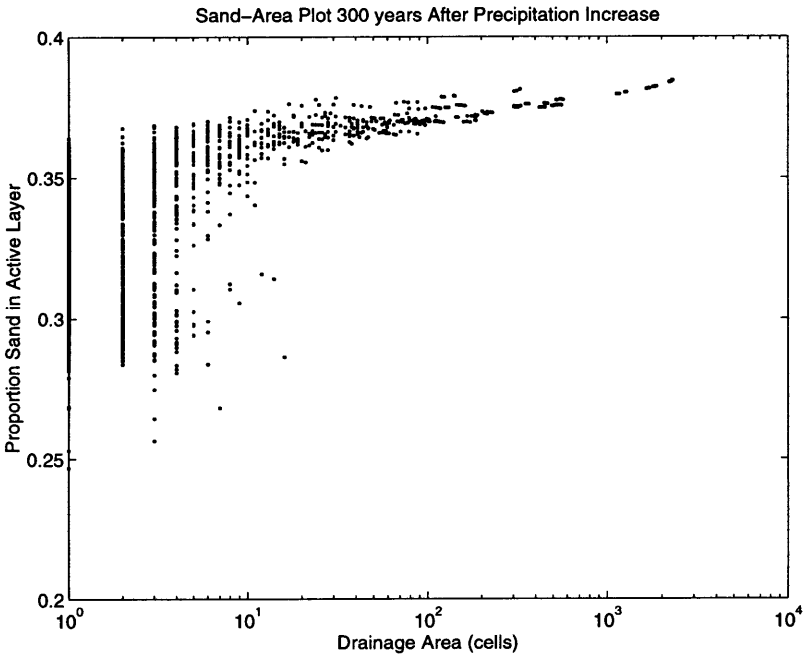

Figure 6-2: Sand-area plots showing the adjustment of the basin to increased precipitation. Figure (a) shows the initial conditions before precipitation was increased. Figures (b), (c), (d), (e), (f) and (g) shows the sand-area plot at six later times after the precipitation increase.

be predicted without knowing the amount of time the system has had to adjust. The complex response in the texture of alluvial deposits could be incorrectly interpreted in a natural system as the response to a multiple changes in climate.

In this example of textural response to climate change, the headwaters and main channels experience different sequences of textural change. Initially erosion caused the active layer in the headwaters to fine. Figure 6-4 (a) shows the elevation and active layer texture changes through time at the top cell in the tributary shown in Figure 6-3. Throughout the entire 180 years shown in the layer plot, the top cell was eroding and the active layer was fining. Figure 6-4 (b) shows the elevation and active layer texture changes through time at the last cell of the tributary shown in Figure 6-3. This cell was aggrading throughout the entire 180 years shown in the layer plot. However, the active layer at this bottom cell first became coarser, then finer, all while the elevation was increasing. The results indicate that there is no direct correlation between changes in the texture of alluvial deposits and erosion or deposition.

The initial slope-area plot and two slope-area plots at later times are shown in Figure 6-5. As the system adjusts, there is some noise in the slope-area plot. In the lower drainage areas slope decreases, in some places by an order of magnitude. In the higher drainage areas slope increases slightly. There is not as much noise in the higher drainage areas as there is in the lower drainage areas. The slope-area plot is less organized at 300 years that it was at 150 years after the increase in precipitation rate, in contrast to the sand-area plot which is relatively more organized 300 years after the increase in precipitation rate than it was 150 years after the increase in precipitation rate. Adjustment of surface texture does not necessarily imply that local slope has adjusted.

6.1.2 Dynamic Equilibrium

Figure 6-6 shows the topography, sand-area and slope-area plots 100,000 years after the increase in precipitation rate, when the system reached a new dynamic equilibrium. Downstream fining was fully re-established. For a given drainage area, the

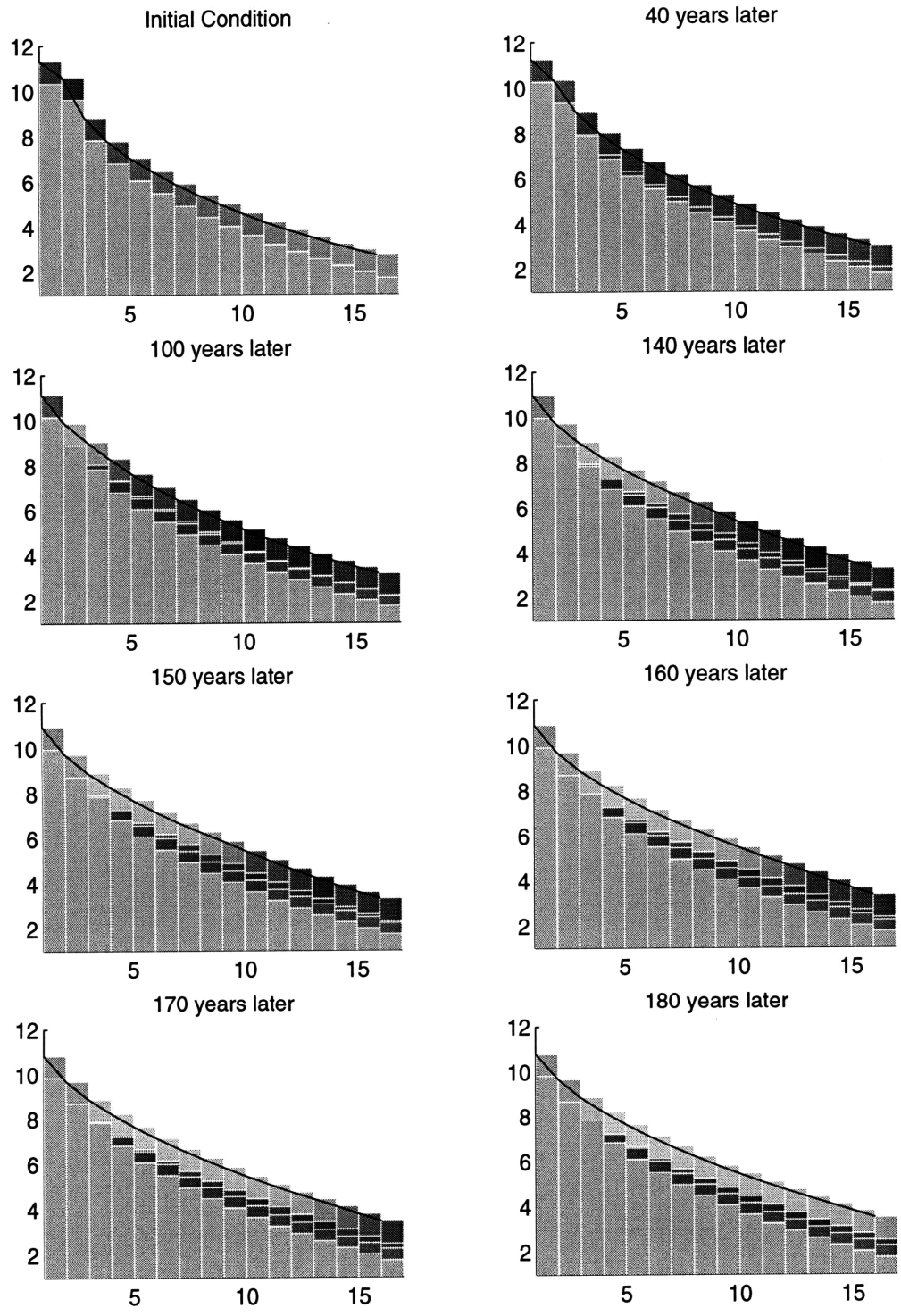

Figure 6-3: The layering through time in a single tributary stream. Dark shading is relatively coarse material, light is relatively fine. All of the plots use the same shading scale. The bottom layer at all nodes is the parent material, composed of 35% sand.

(a)

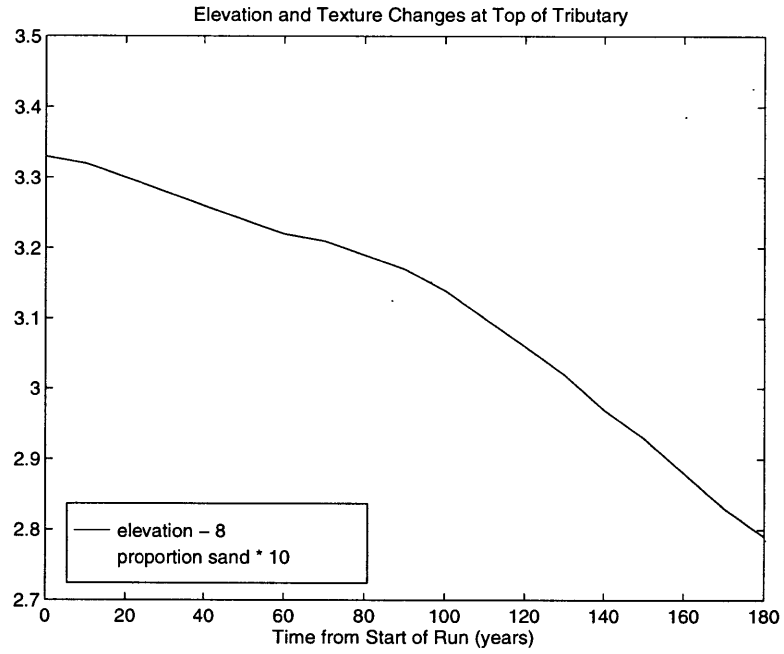

(b)

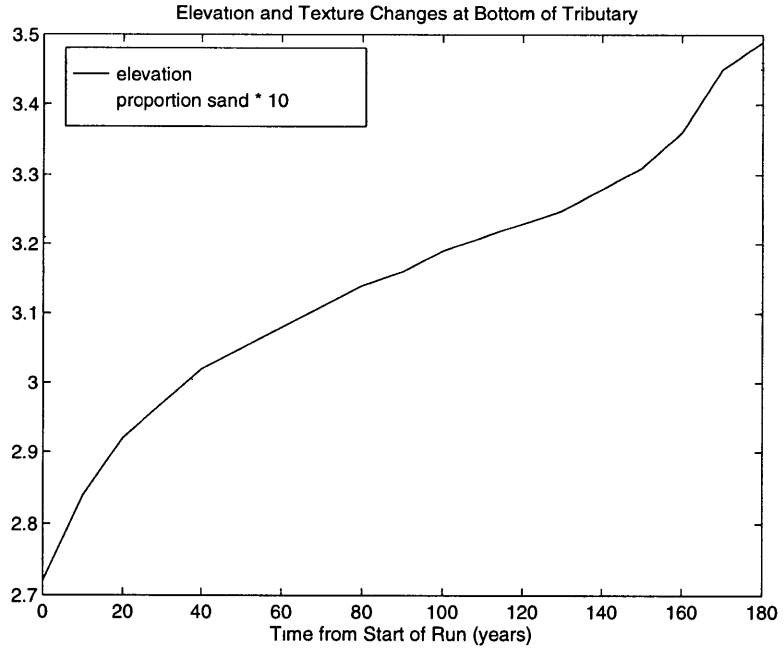

Figure 6-4: Elevation and active layer texture changes through time at two different cells; (a) shows the top cell in the tributary shown in Figure 6-3 and (b) shows the bottom cell.

(a)

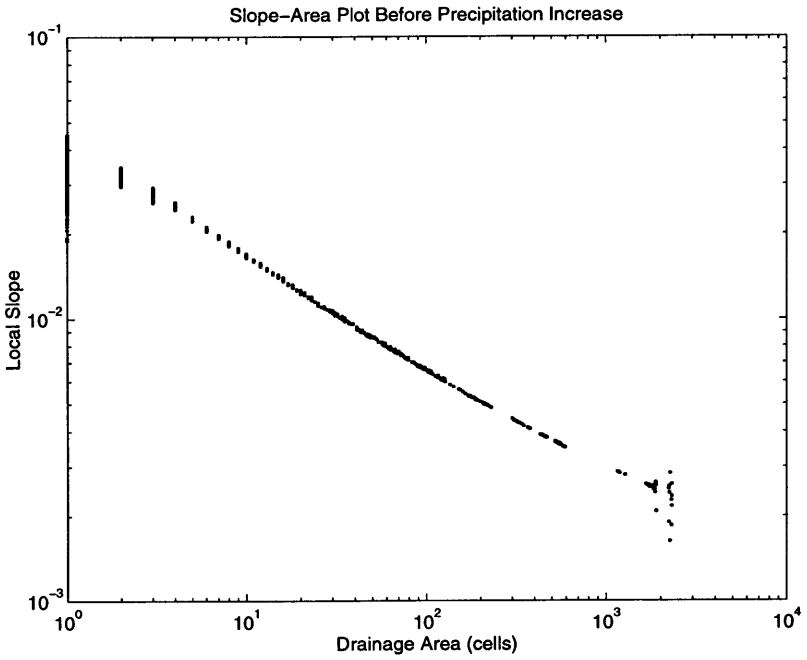
Slope–Area Plot Before Precipitation Increase
Local Slope
Drainage Area (cells)
10^{-1}
10^{-2}
10^{-3}
10^{0}
10^{1}
10^{2}
10^{3}
10^{4}

(b)

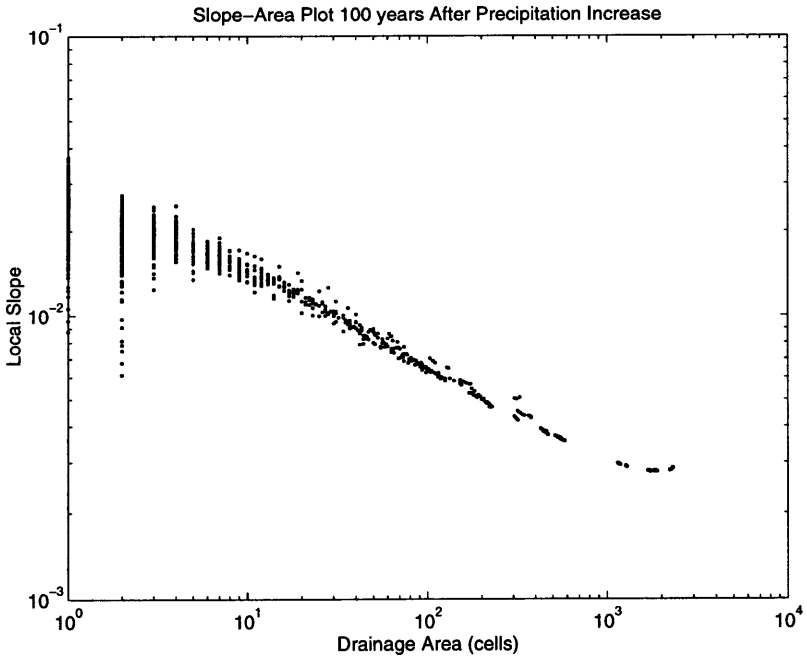
Slope–Area Plot 100 years After Precipitation Increase
Local Slope
Drainage Area (cells)
10^{-1}
10^{-2}
10^{-3}
10^{0}
10^{1}
10^{2}
10^{3}
10^{4}

(c)

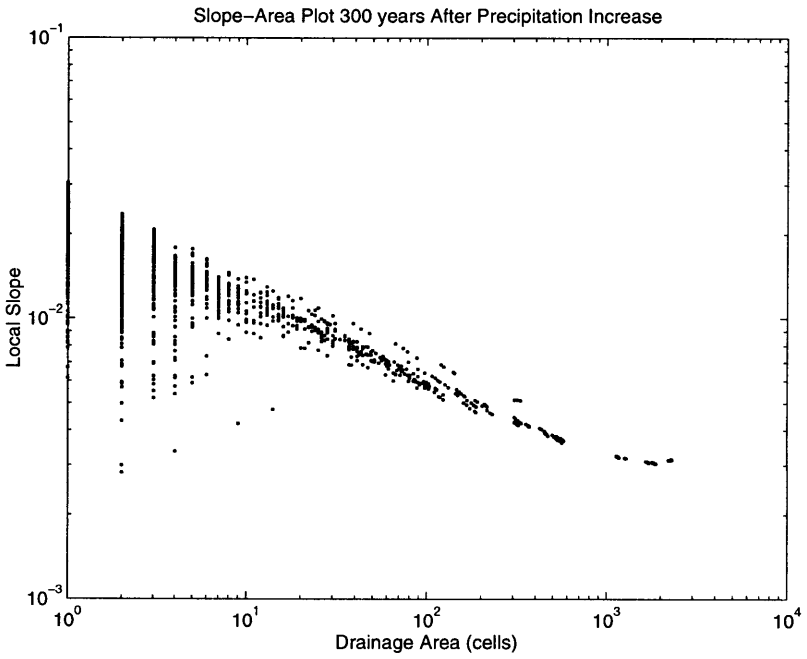

Figure 6-5: Slope-area plots for the basin at three different times. (a) shows the initial slope-area plot before precipitation was increased. (b) and (c) show changes in the slope-area plot at two different times as the basin adjusts to the increased precipitation.

active layer became coarser everywhere than it was at the start of the run. The basin became slightly more concave. Before the increase in precipitation rate, the slope of the slope-area plot is -0.39; after the system establishes a new dynamic equilibrium the slope of the slope-area plot is -0.42. This is contrary to what was expected from the slope-area plots during the initial adjustment of the basin (to the increase in precipitation rate) when concavity was decreasing. The higher concavity is due to the coarser active layer. For a given drainage area the local slope decreased everywhere, and total relief reduced to approximately half of its original value, due to the increase in discharge across the basin.

The basin endured large amounts of adjustment to reach the new equilibrium. The network rearranged itself, and the streams became oriented more towards the outlet than they were initially. The reworking of the network completely erased all of the layers which were deposited during the transient stage.

6.2 Discussion

A number of interesting textural changes result from increasing the precipitation rate in the basin. Downstream fining was disturbed and reversed itself, but only for a short period. When the basin finally reached a new equilibrium, downstream fining was fully re-established. In the new dynamic equilibrium, the active layer, for a given drainage area, coarsened. The pattern of fining remains gradual, because the range of active layer texture is still between 10% and 40% sand (see section 5.1.1).

In the transient stage, signs of the climate change were apparent in the coarse deposits below the active layer. These deposits persisted even after the active layer texture became finer again. The increase in precipitation caused both a coarsening and fining of the surface, suggesting a complex response of the texture of alluvial deposits due to a single climate change. As of yet this result has not been compared with locations which have undergone similar changes in climate, but the model has the potential to become a valuable tool in understanding the effect of climate change on real landscapes.

(a)

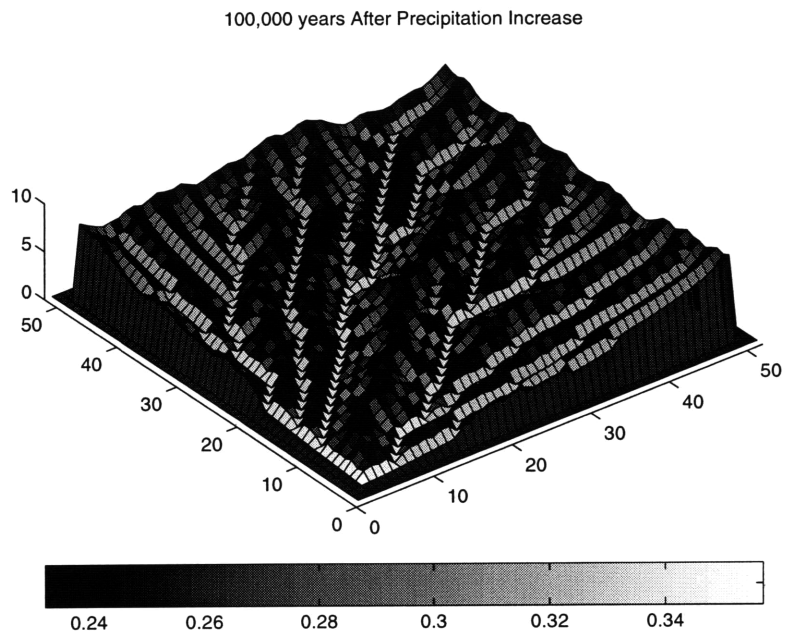
100,000 years After Precipitation Increase
10
5
0
50
40
30
20
10
0
0
10
20
30
40
50
0.24
0.26
0.28
0.3
0.32
0.34

(b)

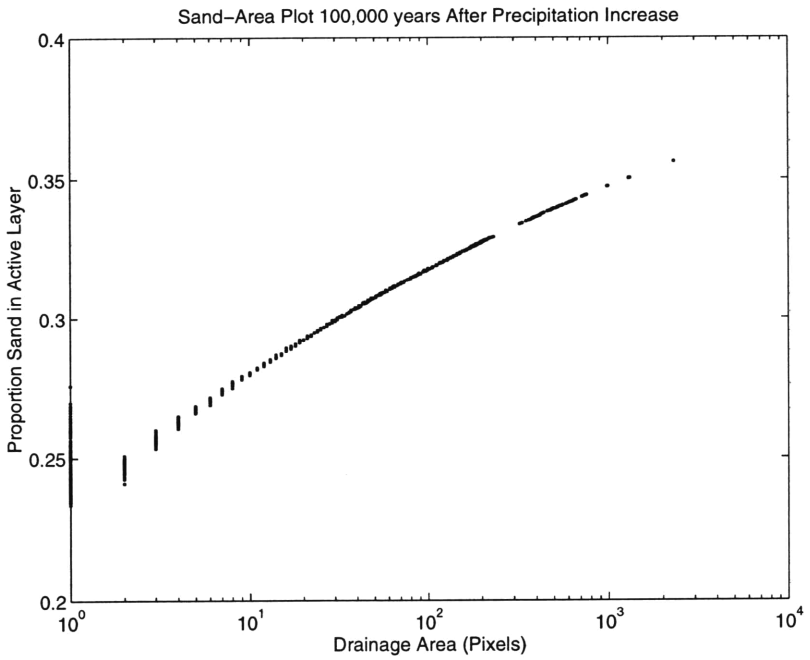
Sand–Area Plot 100,000 years After Precipitation Increase
Proportion Sand in Active Layer
0.4
0.35
0.3
0.25
0.2
10^0
10^1
10^2
10^3
10^4
Drainage Area (Pixels)

(c)

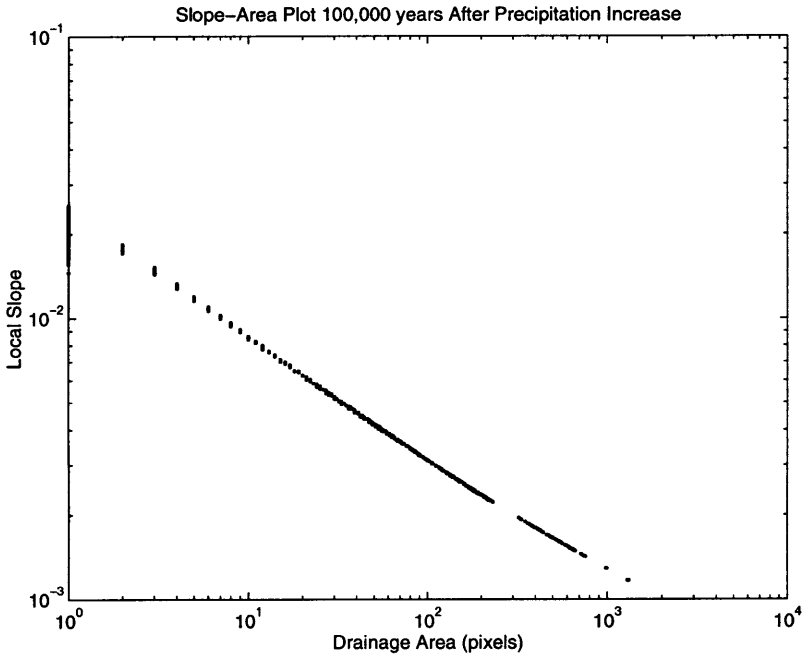

Figure 6-6: Topography (a), sand-area plot (b), and the slope-area plot (c) of the new dynamic equilibrium conditions after precipitation was increased. Note that the colormap has changed from Figures 6-1.

Concavity also changes as a result of the climate change. Initially, erosion of the hillslopes and deposition in the valleys resulted in a decrease in concavity. However, after a long period of adjustment, the end result was a slightly more concave basin. The increased concavity is not surprising because the the active layer coarsened, and active layer texture governs basin concavity. The initial changes in fining and concavity do not necessarily foreshadow the end result of the climate change. This suggests that the transient effects of climate change might be quite different from the long-term effects.

Previous field studies linking climate change and deposit texture have often not been in agreement with one another. Blum and Valastro (1989) examined the response of the Pedernales river (central Texas) to late Holocene climate change. During the late Holocene, the Pedernales River was an aggrading, gravel-dominated stream. Paleoenvironmental data suggests that the climate during the Holocene was wetter than the present climate. The rainfall produced enough runoff to deliver an overabundance of coarse gravel to the main valley. The drier conditions of the present supply less gravel to the main stream, causing the modern Pedernales channel to contain finer-grained, gravel-poor deposits. However, Blum and Valastro (1989) cite previous studies of sedimentary adjustments to climate change which found that coarse-grained sediment loads are present during arid time periods and fine-grained sediment loads are present during humid time periods. They conclude that fluvial systems are extremely sensitive to climatic change. The results of this modeling study suggest that part of this sensitivity may lie in the complex response to climate change.

The modeled basin requires a very long time to completely re-adjust to the change in precipitation rate. Once the basin reaches a new dynamic equilibrium, the signs of the precipitation change are completely erased. Most likely, a natural system would not have this much time to fully adjust to a new climate. Before a new equilibrium is reached, the climate would probably change again. Examination of Greenland ice cores suggests that rapid fluctuations in climate are apparent on the time scale of decades (Taylor et al. 1993). The amount of time a system has to adjust could greatly affect the preservation and texture of alluvial sequences. This study has only brushed

the surface in answering the question of how climate change affects alluvial deposits. Results do imply, however, that fluctuations in both concavity and the texture of alluvial deposits can result from a single change in the effective precipitation rate.

There is still much to be learned from this study. A more careful look at the adjustment of the system between 300 years after the precipitation increase and 100,000 years after the increase will be useful in further understanding the adjustment of the basin. Other tributaries in the basin can be investigated to see whether they all follow the same pattern of deposition and fining after the initial coarsening. The controls on the time scale of both coarsening and fining still need to be investigated.

Chapter 7

Conclusions

7.1 Summary of Results

This study used a physically based numerical model to investigate changes in surface texture throughout a drainage basin. Previous modeling efforts investigating texture changes have all used two-dimensional models. The addition of multiple grain sizes to a three-dimensional basin evolution model brings numerical models one step closer to capturing all of the many complex interactions between different forces in natural landscapes.

An algorithm which creates and destroys sedimentary layers was developed. This allows for more realistic results during erosion when layers of material which were previously deposited are brought to the surface. The user is able to track the texture of sedimentary layers and link them with specific events. This becomes very useful when studying the effects of climate change or any perturbation of the system.

The sensitivity of the model to changes in a single effective grain size was discussed in Chapter 4. The homogeneous basin simulations examined the same premise which was applied in past modeling studies, that a mixture of sediment across the landscape can be represented with one effective grain size. The results show that basin concavity directly depends on the effective grain size. Basins with larger effective grain sizes evolved to become more concave than those with smaller effective grain sizes. Although one would never expect a natural basin to be composed of a single

grain size, reasonable concavity results were obtained with effective grain sizes in the gravel range. However, highly unrealistic morphologies resulted when basins were evolved with an effective grain size in the sand range. All of the effective grain sizes used in the study are reasonable for parts of a natural system. This suggests that using a single grain size misses an important interaction in the system which allows the basin to evolve to a reasonable morphology.

The use of two grain sizes to represent a sediment mixture was discussed in Chapter 5. In the heterogeneous basins, the active layer texture adjusts to become finer as drainage area increases. The nature of the fining in the modeled basins depends on the surface texture. Fining is gradual when there is less than 40% sand in the active layer. Once the active layer texture surpasses 40% sand, fining becomes much more rapid. The change from less than 40% sand to greater than 40% sand represents a change from gravel- to sand-bed stream. This transition is quite abrupt in natural rivers, as it is in the model results. The texture of the substrate controls the location of the transition from gravel- to sand-bed stream. The transition does not take place in all of the modeled drainage basins, but it could if bed shear stress was increased.

The adjustment of the active layer texture plays a large role in basin concavity. All of the basins with different textures of parent material were found to have realistic concavities. The active layer texture governs sediment transport rates which govern basin concavity. In most areas of the different basins the active layer is largely composed of coarse material. This allows for realistic concavity results, even with sand on the bed and in the parent material. In the basin with the finest parent material, a change in concavity is linked to the transition from a predominantly gravel bed to a predominantly sand bed. Many natural rivers exhibit a change in concavity when the bed changes from gravel to sand. The model is able to capture the natural differences between these two types of streams.

The model results regarding downstream fining are unique for two reasons. Selective deposition is usually credited as the main cause of downstream fining. Downstream fining in this study, however, results from the adjustment of the active layer to erosion, not deposition. The results also show that downstream fining can occur

under steady-state conditions. In many previous studies downstream fining has been described as a transient state.

Chapter 6 introduces some of the effects of climate change on alluvial texture. Simply by increasing the effective precipitation rate, the entire pattern of fining goes through multiple stages of adjustment. In the transient state, a pattern of downstream coarsening is observed as the headwaters become finer and the valleys become coarser. The system quickly erases the pattern of coarsening as the valleys become even finer than they were initially, and some of the headwaters still remain fine. In some locations coarse sedimentary deposits remain below the active layer even after it becomes finer again. Eventually the basin reaches a new dynamic equilibrium and re-establishes a pattern of downstream fining. In the new dynamic equilibrium, the active layer is coarser than it was in its original equilibrium before the precipitation rate was increased. In the new equilibrium, the basin is slightly more concave than it was originally. In the transient stage, however, the basin becomes less concave than it was initially. The results indicate that a single change in climate can produce a number of fluctuations in both basin concavity and texture of alluvial sedimentary deposits.

7.2 Future Studies

This experiment demonstrated that climate change is linked with many interesting patterns in sedimentary texture. However, the experiment was only done on a single basin. More experiments of this type could be performed on basins with different parent material textures. The magnitude of the precipitation increase could be explored, as could the effect of a gradual increase in precipitation instead of a step increase. The frequency of climate change could also be investigated. If the precipitation rate is perturbed before a basin reaches equilibrium, the results could be very different. Complex stratigraphic records might be produced, or possibly no stratigraphy at all if the system is not given much time to adjust between perturbations. Variations on the climate change experiment presented in this study might produce very different

results.

A number of changes can be made to the numerical model to improve different processes and assumptions. All sediment is assumed to travel as bedload. In coarse reaches of the system this is a fair assumption, but this assumption is less accurate in the finer parts of the basin. The addition of suspended load should improve the sediment transport calculations and may have an effect on basin concavity. The infinite supply of bedload might be more realistically replaced with bedrock at some depth below the surface. The constant precipitation rate could be replaced with a more realistic representation of storms. Both storm duration and intensity could be modeled. Different storm sizes might affect the composition of the active layer, just as the increase in precipitation did. Vegetation could also be added to the model. Finally, the addition of more than two grain sizes should help capture changes within the sand and gravel parts of the system.

This study has begun to investigate the interactions of multiple grain sizes and their effects on basin concavity. The results of these experiments will be useful in understanding the dynamics of grain size and morphology once further additions are made to the model. The numerous avenues of further study promise many interesting results in the future.

References

Andrews, E. (1983). Entrainment of gravel from naturally sorted riverbed material., *Geological Society of America Bulletin* **94**: 1225–1231.

Armanini, A. (1992). Variation of bed and sediment load mean diameters due to erosion and deposition processes, *in* P. Billi, R. D. Hey, C. R. Thorne and P. Tacconi (eds), *Dynamics of Gravelbed Rivers*, John Wiley and Sons Ltd, pp. 351–359.

Blum, M. D. and Valastro, S. (1989). Response of the Pedernales River of Central Texas to late Holocene climate change, *Annals of the Association of American Geographers* **79**(3): 435–456.

Borah, D. K., Alonso, C. V. and Prasad, S. N. (1982a). Routing graded sediments in streams: Applications, *American Society of Civil Engineers, Journal of the Hydraulics Division* **108**(HY12): 1504–1517.

Borah, D. K., Alonso, C. V. and Prasad, S. N. (1982b). Routing graded sediments in streams: Formulations, *American Society of Civil Engineers, Journal of the Hydraulics Division* **108**(HY12): 1486–1503.

Chow, V. (1959). *Open-channel hydraulics*, McGraw-Hill.

Church, M. (1985). Bed load in gravel-bed rivers: Observed phenomena and implications for computation., Canadian Society for Civil Engineering Annual Conference.

Church, M., Wolcott, J. and Fletcher, W. (1991). A test of equal mobility in fluvial sediment transport behavior of the sand fraction., *Water Resources Research* **27**(11): 2941–2951.

Einstein, H. (1950). The bedload function for sediment transport in open channel flows., *Technical Bulletin 1026*, United States Department of Agriculture, Soil Conservation Service, Washington, D.C.

Ferguson, R., Hoey, T., Wathen, S. and Werritty, A. (1996). Field evidence for rapid downstream fining of river gravels through selective transport, *Geology* **24**: 179–182.

Flint, J. J. (1974). Steam gradient as a function of order, magnitude, and discharge, *Water Resources Research* **10**(5): 969–973.

Hoey, T. B. and Ferguson, R. (1994). Numerical simulation of downstream fining by selective transport in gravel bed rivers: Model development and illustration, *Water Resources Research* **30**: 2251–2260.

Hoey, T. B. and Ferguson, R. I. (1997). Controls of strength and rate of downstream fining above a river base level, *Water Resources Research* **33**(11): 2601–2609.

Ichim, I. and Radoane, M. (1990). Channel sediment variability along a river; a case study of the Siret River, Romania, *Earth Surface Processes and Landforms* **15**: 211–225.

Ijjasz-Vasquez, E. J., Bras, R. L. and Moglen, G. E. (1992). Sensitivity of a basin evolution model to the nature of runoff production and to initial conditions, *Water Resources Research* **28**(10): 2733–2741.

Komar, P. (1987). Selective grain entrainment by a current from a bed of mixed sizes: a reanalysis., *Journal of Sedimentary Petrology* **57**(2): 203–211.

Komar, P. and Li, Z. (1986). Pivoting analyses of the selective entrainment of sediments by shape and size with application to gravel threshold., *Sedimentology* **33**: 425–236.

Kuhnle, R. (1993). Incipient motion of sand-gravel sediment mixtures., *Journal of Hydraulic Engineering* **119**(12): 1400–1415.

Leopold, L. and Maddock, T. (1953). The hydraulic geometry of stream channels and some physiographic implications, *Professional Paper 252*, United States Geological Survey.

Li, Z. and Komar, P. (1986). Laboratory measurements of pivoting angles for applications to selective entrainment of gravel in a current., *Sedimentology* **33**: 413–423.

Milhous, R. (1973). *Sediment transport in a gravel-bottomed stream.*, PhD dissertation, Oregon State University.

Paola, C., Parker, G., Seal, R., Sinha, K., Southard, J. B. and Wilcock, P. R. (1992). Downstream fining by selective deposition in a laboratory flume, *Science* **258**: 1757–1760.

Park, I. and Jain, S. C. (1987). Numerical simulation of degradation of alluvial channel beds, *Journal of Hydraulic Engineering* **113**(7): 845–859.

Parker, G. (1979). Hydraulic geometry of active gravel rivers., *Journal of Hydraulics Division, American Society of Civil Engineering* **105**(HY9): 1185–1201.

Parker, G. (1991a). Selective sorting and abrasion of river gravel. I: Theory, *Journal of Hydraulic Engineering* **117**(2): 131–149.

Parker, G. (1991b). Selective sorting and abrasion of river gravel. II: Applications, *Journal of Hydraulic Engineering* **117**(2): 150–171.

Parker, G. and Klingeman, P. (1982). On why gravel bed streams are paved., *Water Resources Research* **18**(5): 1409–1423.

Parker, G., Klingeman, P. and McLean, D. (1982). Bedload and size distribution in paved gravel-bed streams., *Journal of the Hydraulics Division, Proceedings of the American Society of Civil Engineers* **108**(HY4): 544–571.

Pizzuto, J. E. (1992). The morphology of graded gravel rivers: a network perspective, *Geomorphology* **5**: 457–474.

Rahuel, J. L., Holly, F. M., Chollet, J. P., Belleudy, P. J. and Yang, G. (1989). Modeling of riverbed evolution for bedload sediment mixtures, *Journal of hydraulic engineering* **115**(11): 1521–1542.

Seal, R., Paola, C., Parker, G., Southard, J. and Wilcock, P. (1997). Experiments on downstream fining of gravel: I. Narrow-channel runs, *Journal of hydraulic engineering* **123**(10): 874–884.

Sediment transport geochemestry (1989). Ok Tedi Mining Ltd., Papua New Guinea. Final Report, Sixth Supplemental Agreement Environmental Study, 1986-1988.

Shields, A. (1936). Application of similarity principles and turbulence research to bedload movement., *Technical Report Hydrodanmic Lab. Rep. 167*, California Institute of Technology, Pasadena, Ca.

Tarboton, D. G., Bras, R. L. and Rodriguez-Iturbe, I. (1989). The analysis of river basins and channel networks using digital terrain data, *Technical Report 326*, Massachusetts Institute of Technology, Ralph M. Parsons Laboratory.

Taylor, K. C., Lamorey, G. W., Doyle, G. A., Alley, R. B., Grootes, P. M., Mayewski, P. A., White, J. W. C. and Barlow, L. K. (1993). The 'flickering switch' of late Pleistocene climate change, *Nature* **361**: 432–436.

Tucker, G. E. (1996). *Modeling the large-scale interaction of climate, tectonics, and topography*, PhD thesis, The Pennsylvania State University.

Tucker, G. E. and Bras, R. L. (1997). Hillslope processes, drainage density, and landscape morphology. In review.

van Niekerk, A., Vogel, K. R., Slingerland, R. L. and Bridge, J. S. (1992). Routing of heterogeneous sediments over movable bed: Model development, *Journal of Hydraulic Engineering* **118**(2): 246–261.

Vogel, K. R., van Niekerk, A., Slingerland, R. and Bridge, J. S. (1992). Routing of heterogeneous sediments over movable bed: model verification, *Journal of Hydraulic Engineering* **118**(2): 263–279.

Wiberg, P. and Smith, J. (1987). Calculations of the critical shear stress for motion of uniform and heterogeneous sediments, *Water Resources Research* **23**(8): 1471–1480.

Wilcock, P. (1997). A method for predicting sediment transport in gravel-bed rivers., the Johns Hopkins University.

Wilcock, P. and Southard, J. (1988). Experimental study of incipient motion in mixed-size sediment., *Water Resources Research* **24**(7): 1137–1151.

Willgoose, G., Bras, R. L. and Rodriguez-Iturbe, I. (1989). A physically based channel network and catchment evolution model, *Technical Report 322*, Massachusetts Institute of Technology.

Wolman, M. G. (1955). The natural channel of brandywine creek pennsylvania, *Professional Paper 271*, United States Geological Survey.

Yatsu, E. (1955). On the longitudinal profile of the graded river, *American Geophysical Union Transactions* **36**(4): 655–663.